A Revised Land Surface Parameterization (SiB2) for Atmospheric GCMs. Part I: Model Formulation

Author(s): P. J. Sellers, D. A. Randall, G. J. Collatz, J. A. Berry, C. B. Field, D. A. Dazlich, C. Zhang, G. D. Collelo and L. Bounoua

A Revised Land Surface Parameterization (SiB2) for Atmospheric GCMs.
Part I: Model Formulation

P. J. SELLERS,* D. A. RANDALL,[†] G. J. COLLATZ,* J. A. BERRY,[@] C. B. FIELD,[@] D. A. DAZLICH,[†] C. ZHANG,[†]
G. D. COLLELO,[@] AND L. BOUNOUA[#]

*NASA/GSFC, Greenbelt, Maryland
[†]Department of Atmospheric Science, Colorado State University, Fort Collins, Colorado
[@]Carnegie Institution of Washington, Stanford, California
[#]USRA, NASA/GSFC, Greenbelt, Maryland

ABSTRACT

The formulation of a revised land surface parameterization for use within atmospheric general circulation models (GCMs) is presented. The model (SiB2) incorporates several significant improvements over the first version of the Simple Biosphere model (SiB) described in Sellers et al. The improvements can be summarized as follows:

(i) incorporation of a realistic canopy photosynthesis–conductance model to describe the simultaneous transfer of CO_2 and water vapor into and out of the vegetation, respectively;

(ii) use of satellite data, as described in a companion paper, Part II, to describe the vegetation phenology;

(iii) modification of the hydrological submodel to give better descriptions of baseflows and a more reliable calculation of interlayer exchanges within the soil profile;

(iv) incorporation of a "patchy" snowmelt treatment, which prevents rapid thermal and surface reflectance transitions when the area-averaged snow cover is low and decreasing.

To accommodate the changes in (i) and (ii) above, the original two-layer vegetation canopy structure of SiB1 has been reduced to a single layer in SiB2. The use of satellite data in SiB2 and the performance of SiB2 when coupled to a GCM are described in the two companion papers, Parts II and III.

1. Introduction

The formulation of a revised land surface parameterization for use within atmospheric general circulation models (GCMs) is presented. This new parameterization (SiB2) incorporates several improvements over the first version of the Simple Biosphere model (hereafter referred to as SiB1) of Sellers et al. (1986), including the incorporation of a realistic canopy photosynthesis–conductance submodel and the use of satellite data to describe vegetation state and phenology. The principle motivation for formulating SiB2 was to provide more realistic estimates of sensible and latent heat fluxes over the continents along with consistent estimates of large-scale carbon assimilation rates.

SiB1 used physically based formulations to calculate turbulent transfer and reflectance properties of the vegetated land surface as functions of leaf-area index (LAI), canopy morphology, and vegetation element and soil optical properties. Empirical expressions were used to calculate the canopy transpiration resistance as a function of LAI, vegetation type, and environmental

conditions (light, soil moisture, temperature, humidity). Maps of vegetation type based on the ground-based classification work of Kuchler (1983) and Matthews (1984, 1985) were combined with vegetation phenologies specified from data gathered from a survey of the ecological literature (see Dorman and Sellers 1989) to provide global time series of green LAI and thereafter the parameters mentioned above. This approach yielded some success in that more realistic continental fields of evaporation, sensible heat flux, near-surface air temperature, and precipitation were calculated by GCMs using SiB1 when compared with parallel runs executed using conventional abiological land-surface parameterizations (see, for example, Sato et al. 1989a). However, the empirical canopy conductance calculation and the arbitrary prescription of vegetation phenology were recognized weaknesses of SiB1.

Two scientific developments prompted a radical revision of SiB1 and its associated datasets. First, work carried out in the 1980s and early 1990s by plant physiologists and ecologists provided new insights into the biochemical mechanisms governing photosynthesis and how these are tied to stomatal function (see, for example, Farquhar et al. 1980; Ball 1988; Collatz et al. 1990; Collatz et al. 1991). Further work by Field

Corresponding author address: Dr. Piers J. Sellers, Biospheric Sciences Branch/NASA/GSFC, Code 923, Greenbelt, MD 20771.

(1983) and Field and Mooney (1986) and others showed how vegetation canopies distributed biochemical resources so as to maximize their photosynthetic efficiency. Sellers et al. (1992a) integrated the new photosynthesis–conductance models using these ecological efficiency principles to produce a physiologically plausible canopy-scale photosynthesis–conductance model.

Second, optical remote sensing of the land surface matured during the 1980s as a result of global diagnostic studies using satellite data (Tucker et al. 1986); plot-scale field studies (Asrar et al. 1984; Tucker et al. 1981); large-scale field experiments (Sellers et al. 1992b; Hall et al. 1992); and theoretical work (Myneni et al. 1992; Hall et al. 1990; Sellers 1985, 1987; Sellers et al. 1992a). It was shown that satellite observations of the surface in the visible and near-infrared wavelengths could be combined into spectral vegetation indices (SVIs) to provide useful estimates of the fraction of photosynthetically active radiation (0.4–0.7 μm) absorbed by the green part of the vegetation canopy (FPAR). This FPAR term can be directly applied in the integrated canopy photosynthesis–conductance model of Sellers et al. (1992a) to calculate photosynthesis and transpiration over large areas (see Sellers et al. 1992c). These two new developments complement each other perfectly; the more realistic canopy process models (which actually require fewer parameters than the highly empirical physiological models used in SiB1) can be applied globally using satellite spectral vegetation index (SVI) data to define the time–space variations in vegetation activity. At a stroke, the two major weaknesses of SiB1, the empirical canopy conductance model and the arbitrary prescription of vegetation phenology, could be mitigated.

These and a number of other changes made to SiB1 to create SiB2 can be summarized as follows:

(i) A realistic photosynthesis–conductance model is incorporated to describe the simultaneous transfers of CO_2 and water vapor into and out of the leaf, respectively.

(ii) Satellite data is used to describe the vegetation phenology. Simple ratio vegetation index (SR) data acquired from the Advanced Very High Resolution Radiometer (AVHRR) sensor on the NOAA series of meteorological satellites were processed to derive time-series fields of the fraction of photosynthetically active radiation absorbed by the green vegetation canopy (FPAR), the total LAI (L_T), and the canopy greenness fraction (N). FPAR is used directly in the photosynthesis–conductance calculation, while L_T is used in the specification of land surface turbulent transfer and reflectance properties.

(iii) The hydrological submodel is modified to give better descriptions of base flows and a more reliable calculation of interlayer exchanges within the soil profile.

(iv) A "patchy" snowmelt description is incorporated that prevents rapid thermal transitions when the area-averaged snow cover is low and decreasing.

To accommodate the changes described in (i) and (ii), the two-layer canopy structure used in SiB1 was reduced to a single vegetation layer in SiB2.

These improvements are reviewed in this paper. A companion paper, Sellers et al. (1996), describes the new datasets used by SiB2, in particular those data derived from satellite observations. A third paper, Randall et al. (1996), describes the performance of the coupled SiB2-GCM combination. In this form, SiB2-GCM calculates the conventional land-surface–atmosphere fluxes of radiation, momentum, and sensible and latent heat. In the process, the models calculate the global-scale uptake of carbon by terrestrial plants in photosynthesis, that is, gross primary productivity (GPP).

2. Sensitivity of the climate system to the state of the land surface

A number of sensitivity studies were carried out in the late 1970s and early 1980s using abiological land surface parameterizations (LSPs) to explore the roles of albedo, surface roughness, and moisture availability in GCM climatologies (see the review of Garratt 1993). Recent work with biophysically realistic models has focused on the role of vegetation and soil type on continental hydrometeorology. Some of the most important findings are summarized below.

(i) Improved simulation of continental hydrometeorology: Sato et al. (1989a) compared the results of a SiB2-GCM run with those obtained with a conventional bucket hydrology model (control). The continental evaporation rates associated with the SiB1 simulation were consistently lower and in closer agreement with the available observations compared with the results from the control run, mainly because of the specification of a surface (stomatal) resistance term to water vapor transfer in SiB1. The reduced evapotranspiration rates in SiB1 resulted in reduced and more realistic continental precipitation fields. More recently, Betts et al. (1994) showed how the implementation of an improved soil moisture and surface resistance parameterization in a numerical weather prediction model resulted in a greatly improved simulation of the precipitation anomaly that gave rise to the Midwestern floods in the United States in the summer of 1993.

(ii) Improved realism of "land cover change" simulation experiments: Dickinson and Henderson-Sellers (1988), Lean and Warrilow (1989), and Nobre et al. (1991) all used biophysically based models to study the impact of large-scale Amazonian deforestation on the regional and global climate. The results from the latter two studies are consistent in showing decreases in regional evapotranspiration and precipitation linked to increases in surface temperature of around 3–5 K associated with the deforestation case. Xue and Shukla

(1991) used SiB1 to investigate the influence of vegetation on precipitation patterns in the Sahelian regional of Africa. They found that replacement of seasonal forest and grassland by desert led to a simulated reduction in evapotranspiration and rainfall over the same areas, resulting in a net displacement of the seasonal rainfall patterns to the south.

(iii) Improved understanding of the effects of spatial or temporal variations in land surface properties: Koster and Suarez (1994) used a variant of SiB1 to investigate the effects of diurnal variations in surface resistance on convective precipitation rates over the continents. In SiB1, the empirical canopy physiological model acts to increase surface resistance as the near-surface vapor pressure deficit increases during the afternoon. This effect, which is observed in nature and is assumed to be a water-conserving mechanism in higher plants, reduces afternoon evapotranspiration rates and increases sensible heat fluxes above the levels calculated with diurnally constant surface resistance values: convection and convective rainfall rates are significantly enhanced as a result. Koster and Suarez (1992) also used SiB1 to calculate the contributions of "mosaics" of different vegetation types within a single GCM grid square to explore different averaging schemes; it was found that some straightforward averaging of key parameters could produce results comparable to fully discretized treatments. Noilhan et al. (1991) and Pielke and Avissar (1990) used biophysical LSPs within mesoscale models to explore the role of vegetation type and/or soil moisture discontinuities on mesoscale circulations and their contributions to area-averaged heat and moisture fluxes. Their work and reports from other groups indicate that sharp variations in land surface properties, for example, forest-agriculture boundaries, can give rise to significant mesoscale effects under certain conditions.

The need for enhanced realism and accuracy in all aspects of climate modeling will increase as scientists try to understand and predict the implications of global change. Up to now, the emphasis has been on improving the calculation of the surface energy and water budgets in LSPs since these are associated with fluxes that have immediate and large effects on the physical climate system as represented in GCMs. However, we anticipate that there will be a significant demand for realistic representation of longer timescale processes, notably the carbon cycle and large-scale hydrology, in earth system models of the future.

3. Modeling strategy

SiB1 of Sellers et al. (1986) and BATS of Dickinson (1984) were based on a biophysical approach to modeling the surface energy and moisture balance, in large part using methodologies developed by micrometeorologists and agricultural scientists as reviewed in Monteith (1973), for example. In SiB1, vegetation param-

eters were used within submodels for radiation, momentum, and heat-mass transfer to calculate the albedo, roughness, and surface resistance of a given GCM grid area. The radiation and turbulent transfer components of SiB1 are covered in Sellers et al. (1986) and are reviewed later in this paper and in the appendices.

The most obvious weakness of SiB1 was connected with the formulations used to describe the biophysical control of evapotranspiration. The empirical leaf-level model of Jarvis (1976) describes leaf stomatal resistance as a function of incident photosynthetically active radiation (PAR, effectively equivalent to visible radiation), temperature, vapor pressure deficit, and leaf-water potential. Sellers (1985) integrated this model to account for variations in PAR flux within a vegetation canopy as a result of leaf position and orientation to give an estimate of the bulk canopy resistance for SiB1. The effects of soil moisture stress, which are expressed through a leaf-water potential term, were accounted for by a soil-water extraction model following Federer (1979). Soil evaporation was handled by an isothermal diffusion model. The parameters required for the surface (canopy) resistance model were LAI, leaf optical properties, leaf orientation, and a large number of species-specific physiological parameters, all of which are highly empirical and defined from a very sparse collection of measurements (see Sellers et al. 1986; Dorman and Sellers 1989).

The empirical species-specific canopy resistance formulation and the specification of global times-series fields of LAI, etc., from in situ observations were known to be large sources of uncertainty. SiB2 includes two major improvements over SiB1 to address these shortcomings.

(i) *Incorporation of more realistic leaf- and canopy-scale models of photosynthesis–conductance.*

Here the aim was to make use of more realistic, less empirical models that would also require the specification of a much smaller set of physiological parameters.

Farquhar et al. (1980) presented a biochemical model of leaf photosynthesis, subsequently extended by von Caemmerer and Farquhar (1985) and other researchers, which describes CO_2 assimilation A, by chloroplasts or leaves as rate-limited by enzyme kinetics, specifically the amount and cycle time of the carboxylating enzyme Rubisco, and by electron transport, which is a function of incident PAR and the efficiency of the leaf's light-intercepting apparatus (chlorophyll). Collatz et al. (1991) present details of a mature version of this model for C_3 vegetation, which accounts for around 80% of the world's vegetation cover, including all forests and temperate grasses. A modification of the model for C_4 vegetation (principally tropical grasses) may be found in Collatz et al. (1992).

Sellers et al. (1992a) integrated the leaf-level model of Collatz et al. (1991) over a vegetation can-

TABLE 1. Principal variables and parameters used in SiB2: (a) atmospheric boundary conditions, (b) time-invariant parameters, (c) time-varying parameters, (d) soil physical properties, and (e) prognostic variables.

Symbol	Definition	Unit	Symbol	Definition	Unit
(a) Atmospheric boundary conditions				physiological properties (*continued*)	
T_m	atmospheric boundary-layer temperature	K	S	rubisco specificity for CO_2 relative to O_2	—
e_m	atmospheric boundary-layer vapor pressure	Pa	K_c	Michaelis–Menten constant for CO_2	Pa
			K_o	inhibition constant for O_2	Pa
u_m	atmospheric boundary-layer wind speed	m s^{-1}	ϵ_3, ϵ_4	intrinsic quantum efficiency of C_3, C_4 photosynthesis	mol mol^{-1}
c_m	atmospheric boundary-layer CO_2 partial pressure	Pa			
			β_{ce}, β_{ps}	coupling coefficients	—
o_m	atmospheric boundary-layer O_2 partial pressure	Pa	f_d	leaf respiration coefficient	—
			m	stomatal slope factor	—
z_m	atmospheric boundary-layer reference height	m	b	minimum stomatal conductance	mol m^{-2} s^{-1}
$F_{\Lambda,\mu(0)}$	incident solar radiation, Λ = V (visible), N (near infrared), μ = d (diffuse), b (beam)	W m^{-2}	$s_1, s_3,$ s_5	temperature inhibition parameters	K^{-1}
			$s_2, s_4,$ s_6	half-inhibition temperature parameters	K
$F_{T,d(0)}$	incident thermal infrared radiation (diffuse only)	W m^{-2}	ψ_c	half-inhibition water potential parameter	m
P_c	convective precipitation rate	mm	**(c) Time-varying parameters**		
P_p	large-scale precipitation rate	mm	FPAR	fraction of incident radiation absorbed by green canopy	—
p	atmospheric surface pressure	Pa			
			L_T	total leaf-area index	m^2 m^{-2}
(b) Time-invariant vegetation parameters			N	canopy greenness fraction	—
			z_0	canopy roughness length	m
morphological properties			d	canopy zero plane displacement	m
z_2	height of canopy top	m	C_1	bulk boundary-layer resistance coefficient	(s m$^{-1})^{1/2}$
z_1	height of canopy bottom	m			
z_c	inflection height for leaf-area density	m	C_2	ground to canopy air-space resistance coefficient	—
z_s	ground roughness length	m			
V	canopy cover fraction	—	$\bar{k}$	mean canopy extinction coefficient	—
χ_L	leaf-angle distribution factor	—	δ_T	canopy thermal infrared transmittance	—
G_1, G_4	momentum transfer coefficient parameters	—	**(d) Soil physical properties**		
l_w, l_l	leaf width, length	m	ψ_s	soil water potential at saturation	m
D_1	depth of surface soil layer (0.02)	m	K_s	soil hydraulic conductivity at saturation	m s^{-1}
D_r	root depth ($D_1 + D_2$)	m	B	soil wetness parameter	—
D_T	total soil depth ($D_1 + D_2 + D_3$)	m	θ_s	soil water content at saturation (porosity)	m^3 m^{-3}
$\varnothing_s$	mean topographic slope	radians	**(e) Prognostic variables**		
optical properties			T_c	canopy temperature	K
$\alpha_{\Lambda,a}$	leaf reflectance, Λ = V (visible), N (near infrared), a = l (live), d (dead)	—	T_g	soil surface temperature	K
			T_d	deep soil temperature	K
$\delta_{\Lambda,a}$	leaf transmittance, Λ = V (visible), N (near infrared), a = l (live), d (dead)	—	M_{cw}	canopy interception liquid water store	m
			M_{cs}	canopy interception snow–ice store	m
$a_{s,\Lambda}$	soil reflectance, Λ = V (visible), N (near infrared)	—	M_{gw}	soil interception liquid water store	m
			M_{gs}	soil interception snow–ice store	m
physiological properties			W_1	surface soil wetness	—
			W_2	root zone soil wetness	—
V_{max0}	maximum rubisco capacity at canopy top	mol m^{-2} s^{-1}	W_3	deep soil wetness	—
O_2	partial pressure of oxygen in leaf interior	Pa	g_c	canopy conductance to water vapor	m s^{-1}

opy, taking into account the attenuation of PAR and the corresponding exponential decrease in photosynthetic capacity with canopy depth (increasing LAI). It was found that the photosynthetic rate and conductance of an entire canopy could be estimated by multiplying a calculation of the performance of the uppermost leaves in the canopy by a canopy PAR-use parameter Π = FPAR/$\bar{k}$, where FPAR is the fraction of incident PAR absorbed by the green portion of the canopy, and $\bar{k}$ is the canopy extinction coefficient for PAR. Both FPAR and $\bar{k}$ are time-

mean, radiation-weighted quantities. FPAR is the vegetation property that is most amenable to remote sensing (see Sellers et al. 1995; Hall et al. 1992).

(ii) Global specification of the green LAI from satellite remote sensing data.

Satellite platforms offer the only opportunity to specify vegetation parameters almost continuously, worldwide, using consistent instrumentation and data processing techniques. Satellite, airborne, and surface-

TABLE 2. Vegetation classification schemes used in SiB1 and SiB2.

SiB1		SiB2	
Type	Name	Type	Name
1	Broadleaf-evergreen trees	1	Broadleaf-evergreen trees
2	Broadleaf-deciduous trees	2	Broadleaf-deciduous trees
3	Broadleaf and needleleaf trees	3	Broadleaf and needleleaf trees
4	Needleleaf-evergreen trees	4	Needleleaf-evergreen trees
5	Needleleaf-deciduous trees	5	Needleleaf-deciduous trees
6	Broadleaf trees with groundcover	6	Short vegetation/C4 grassland
7	Groundcover	6	Short vegetation/C4 grassland
8	Broadleaf shrubs with groundcover	6	Short vegetation/C4 grassland
9	Broadleaf shrubs with bare soil	7	Broadleaf shrubs with bare soil
10	Dwarf trees and shrubs	8	Dwarf trees and shrubs
11	No vegetation: bare soil	6	Short vegetation/C4 grassland
12	Broadleaf deciduous trees with winter wheat	9	Agriculture/C3 grassland

based sensors have been used to measure upwelling spectral radiances over natural surfaces for around two decades. In particular, spectral vegetation indices (SVIs) have been used as indicators of vegetation density and vigor: SVIs are based on the large difference between the visible and near-infrared reflectances of green leaves as compared to the relatively uniform spectra of soil and rock surfaces.

Tucker et al. (1981), Asrar et al. (1984), Hall et al. (1992), and others have shown that SVI are correlated to field measurements of LAI and FPAR. Theoretical work by Sellers (1985, 1987), Myneni et al. (1992), Hall et al. (1990), and Sellers et al. (1992a) has further demonstrated that there are sound biophysical reasons for these relationships. The work of Sellers (1987) and Sellers et al. (1992a) indicates that the sensor wavebands on the Advanced Very High Resolution Radiometers (AVHRR) mounted on the NOAA series of polar-orbiting satellites are well-suited for providing SVI values that should be near-linearly related to FPAR under a wide range of conditions.

Since the relationships between SVI and FPAR and between FPAR and canopy conductance g_c and photosynthesis A_c are linear or near-linear, an area-averaged value of SVI may be used to provide area-integrated estimates of FPAR, A_c, and g_c (see Sellers et al. 1992a,c).

The incorporation of this new canopy photosynthesis–conductance model with its most critical parameter, FPAR, derived from satellite observations represents the major improvement in SiB2 over SiB1. Subsequent sections provide the details of this and other formulation changes.

4. The model structure

This section describes the atmospheric boundary conditions, the morphological, physiological, and physical parameters, the prognostic variables, and the governing equations of SiB2. The variables and parameters are summarized in Table 1. The overall model structure is shown in Figs. 1 and 2.

a. Atmospheric boundary conditions

The atmospheric boundary conditions necessary to force SiB2 are listed in Table 1a and include the following:

(i) Air temperature T_m, vapor pressure e_m, wind speed u_m, and CO_2 and O_2 concentration c_m and o_m at a reference level, z_m, within the atmospheric boundary layer. In practice, mean values of c_m and o_m can be defined (35 and 2090 Pa, respectively) for current atmospheric conditions.

(ii) Components of the incident radiation $F_{\Lambda,\mu(0)}$: visible (direct and diffuse), near-infrared (direct and diffuse), and thermal (diffuse only) components of the incident radiative flux.

(iii) Convective P_c and large-scale P_l precipitation rates: a simple formula is used in SiB2 to distribute convective rainfall nonuniformly within a grid area. Large-scale precipitation is assumed to be spatially uniform.

b. Time-invariant vegetation and ground parameters

SiB1 had two vegetation layers. It was necessary to reduce these to one layer in SiB2 to incorporate the iterative photosynthesis–conductance model (see section 7) and to make use of satellite data to describe surface parameters (see Sellers et al. 1996). Table 2 shows how this was done: vegetation types 6, 7, 8, and 11 in SiB1 (savannah, perennial grassland, shrubs with grassland, and bare soil–desert, respectively) were assigned properties associated with a single vegetation type in SiB2, C_4 grassland, which is assumed to be the dominant vegetation type in these areas. Note that since vegetation density is specified from satellite data in SiB2, the assignment of a vegetation type to a "pure desert" area is almost irrelevant since it will have no significant vegetation cover specified there anyway. The agricultural areas (winter wheat and broadleaf trees) in SiB1 were assigned properties associated with a C_3 grassland–agriculture cover. These changes also

TABLE 3. Governing equations for SiB2 prognostic variables.

a. *Canopy, ground surface, and deep soil temperatures (T_c, T_g, and T_d)*

Canopy:

$$C_c \frac{\partial T_c}{\partial t} = Rn_c - H_c - \lambda E_c - \xi_{cs}, \qquad (1)$$

soil surface:

$$C_g \frac{\partial T_g}{\partial t} = Rn_g - H_g - \lambda E_g - \frac{2\pi C_d}{\tau_d}(T_g - T_d) - \xi_{gs}, \qquad (2)$$

deep soil:

$$C_d \frac{\partial T_d}{\partial t} = \frac{1}{2(365\pi)^{1/2}}(Rn_g - H_g - \lambda E_g), \qquad (3)$$

where:

T_c, T_g, T_d = temperature (K);
Rn_c, Rn_g = absorbed net radiation (W m^{-2});
H_c, H_g = sensible heat flux (W m^{-2});
E_c, E_g = evapotranspiration rates (kg m^{-2} s^{-1});
C_c, C_g, C_d = effective heat capacities (J m^{-2} K^{-1});
λ = latent heat of vaporization (J kg^{-1});
τ_d = daylength (s);
ξ_{cs}, ξ_{gs} = energy transfers due to phase changes in M_c and M_g, respectively (W m^{-2}).

The subscript "*c*" refers to the canopy, "*g*" to the soil surface, "*d*" to the deep soil.

b. *Interception stores*

Here

$$\frac{\partial M_{cw,s}}{\partial t} = P - D_d - D_c - E_{ci}/\rho_w, \qquad (4)$$

$$\frac{\partial M_{gw,s}}{\partial t} = D_d + D_c - E_{gi}/\rho_w, \qquad (5)$$

where

$M_{cw,s}$, $M_{gw,s}$ = water or snow–ice stored on the canopy or ground (m);
P = precipitation rate (m s^{-1}),
    = $P_c + P_l$;
D_d = canopy throughfall rate (m s^{-1});
D_c = canopy drainage rate (m s^{-1});
E_{ci}, E_{gi} = evaporation rate from interception stores (kg m^{-2} s^{-1});
ρ_w = density of water (kg m^{-3}).

c. *Soil moisture stores*

Here

$$\frac{\partial W_1}{\partial t} = \frac{1}{\theta_s D_1}\left[P_{W_1} - Q_{1,2} - \frac{1}{\rho_w}E_{gs}\right], \qquad (6)$$

$$\frac{\partial W_2}{\partial t} = \frac{1}{\theta_s D_2}\left[Q_{1,2} - Q_{2,3} - \frac{1}{\rho_w}E_{ct}\right], \qquad (7)$$

$$\frac{\partial W_3}{\partial t} = \frac{1}{\theta_s D_3}[Q_{2,3} - Q_3], \qquad (8)$$

where

W_1, W_2, W_3 = soil moisture wetness in the three soil layers,
    = θ_i/θ_s;
θ_i = volumetric soil moisture in layer i (m^3 m^{-3});
θ_s = value of θ at saturation (m^3 m^{-3});
D_i = thickness of the soil layer (m);
$Q_{i,i+1}$ = flow between i and $i + 1$ layers (m s^{-1});
Q_3 = gravitational drainage from recharge soil moisture store (m s^{-1});
P_{W_1} = infiltration of precipitation into the upper soil moisture store (m s^{-1});
    = $D_c + D_d - Ro_1$
Ro_1 = infiltration excess surface runoff rate (m s^{-1}).

d. *Canopy conductance to water vapor*

Here

$$\frac{\partial g_c}{\partial t} = -k_g(g_c - g_{c_{inf}}), \qquad (9)$$

where

g_c = canopy conductance (m s^{-1});
k_g = time constant (s^{-1});
$g_{c_{inf}}$ = Estimate of g_c at $t \to \infty$ (m s^{-1}).

involved some adjustments in the areas occupied by the newly specified C_4 and C_3 grassland–agricultural covers (see text and figures in Sellers et al. 1996). The net result of these changes is that there are now effectively only nine vegetation types in SiB2, all of which have only one story. This simplification reduces the realism of SiB2 in areas that in nature have two-story vegetation covers, such as savannah where C_3 trees overlie C_4 grasslands.

The root and soil models of SiB2 are much the same as in SiB1; see Fig. 1. The roots are assumed to access the soil moisture from the second layer of a three-layer soil model, while the third layer acts as a source for hydrological baseflow and upward recharge of the root zone. The uppermost thin soil layer can act as a significant source of direct evaporation when moist.

Each vegetation type is assigned a set of time-invariant parameters (see Table 1b). These include (i) morphological parameters: canopy height, leaf dimensions, leaf-angle distribution functions, root depths, etc.; (ii) optical properties: phytoelement (leaves and stems) reflectance, and transmittance values for live and dead phytoelements; and (iii) physiological properties, which are mainly connected with the functioning of the photosynthesis–conductance model. These properties are treated as constants for each vegetation type. Within the GCM, time-varying quantities may be combined with these parameters to produce further quantities; for example, the time-varying canopy greenness fraction N is used with the time-invariant phytoelement reflectance and transmittance parameters to generate mean canopy optical property values for a given day and grid area (see section 5).

c. Time-varying vegetation parameters

Table 1c lists the time-varying vegetation parameters used in SiB2. These are generated from satellite data using the methods described in Sellers et al. (1996) and include the fraction of photosynthetically active radiation absorbed by the canopy FPAR, that is, by NL_T, total leaf-area index L_T, the canopy greenness fraction N, and the aerodynamic parameters defined in section 6.

d. Soil physical properties of SiB

In SiB1, soil properties were assigned to each vegetation type in much the same way as the time-invariant vegetation properties listed in Table 1c. However, soil properties exhibit regional variations that can be independent of vegetation type, and vice versa. This became apparent in SiB1 when a single soil type and associated parameter set was assigned to all desert areas in the world. This resulted in an overestimation of the albedo of the deserts of Australia and Northwest America, which had been assigned high soil reflectance values representative of the Sahara. In SiB2, the Food and Agriculture Organization (FAO) global soil-type map

as presented by Zobler (1986) was combined with a table of soil properties to produce global fields of the soil physical properties Ψ_s, K_s, B, θ_s, listed in Table 1d (see also Sellers et al. 1996). Soil optical properties are still assigned by vegetation type by default; however, the satellite-based surface reflectance dataset of Harrison et al. (1990) is applied in desert areas (see Sellers et al. 1996). Soil-layer depths are defined as a function of vegetation type.

e. Prognostic physical state variables of SiB2 and their governing equations

SiB2 has eleven prognostic physical state variables: three temperatures (canopy temperature T_c, soil surface temperature T_g, deep soil temperature T_d); two interception water stores (canopy water M_{cw}, soil surface M_{gw}); two interception snow/ice stores (M_{cs}, M_{gs}); three soil moisture wetness values (W_1, W_2, and W_3); and one prognostic (time stepped) value of canopy conductance [$g_c(=1/r_c)$]. The governing equations, (1) through (9), for these variables are shown in Table 3.

The evapotranspiration from the canopy E_c has two components (i) E_{ci}, evaporation of water from snow/ice or water intercepted by the canopy and (ii) E_{ct}, transpiration of soil water extracted by the root system and lost from the dry fraction of the canopy. Similarly, evaporation from the soil surface consists of (i) E_{gi}, loss from snow/ice and "puddled" water held on the soil surface, and (ii) E_{gs}, evaporation of soil moisture from within the top soil layer.

In (4) and (5) in Table 3, the canopy or ground interception stores in a grid area are either in snow/ice or in liquid water forms prior to precipitation interception. If the precipitation is in a different phase from the stored water, a calculation of phase changes and substrate temperature changes ensues; if snow/ice and liquid water coexist after this calculation, the liquid water is lost to drainage, runoff, or infiltration (see section 8 of this paper). Also in (4) and (5), evaporation losses from snow/ice take into account the extra energy required for sublimation [see (33)].

The use of (9) in Table 3 has two advantages over the conventional steady-state calculations for g_c described by Collatz et al. (1991) and Sellers et al. (1992a). It produces a realistic lag in stomatal response and is computationally far more efficient as it eliminates one complete iterative loop (see appendix C).

In the numerical solution of the prognostic equations for T_c and T_g, we make use of the fact that the heat capacity terms, C_c and C_g, are small relative to the energy fluxes R_n, H, and λE. This makes (1) and (2) "fast" response equations so that changes in T_c and T_g even over a short time step of a few minutes can have a significant feedback on the magnitude of the calculated energy fluxes.

The energy fluxes R_n, H, and λE and the assimilation rate A are explicit functions of (i) the atmospheric

boundary conditions (see Table 1a); (ii) the prognostic variables of SiB2 (see Table 1e); (iii) the three aerodynamic resistances r_a, r_b, and r_d; and (iv) the two surface resistances r_c ($=1/gc$) and r_{soil} ($=1/g_{soil}$) (see Fig. 2). These fluxes are involved in a backward-differencing scheme to calculate the changes in T_c and T_g over a time step Δt. After that, the various moisture fluxes predicted by the model are used to update the moisture stores: $M_{cw,s}$, $M_{gw,s}$, and W_2, W_2, and W_3 (see section 10).

The resistance formulation describes fluxes of heat, water, and CO_2 in the electrical analog form:

$$\text{flux} = \frac{\text{potential difference}}{\text{resistance}}.$$

For the fluxes of sensible heat H_c and H_g, latent heat λE_c and λE_g, and CO_2 (A_c and soil CO_2 flux R_{soil}), the potential differences are represented by temperatures, vapor pressures, and CO_2 partial pressures, respectively. The resistances are equivalent to the integrals of inverse conductances over a path between the specified potential difference endpoints (see Fig. 2). Figure 2a shows how sensible heat fluxes from the canopy and ground must traverse the aerodynamic resistances r_b or r_d and r_a. Canopy water vapor and CO_2 fluxes must traverse an additional resistance r_c ($=1/g_c$), which has a different value for water vapor and CO_2 because of the different diffusion coefficients associated with each (see Figs. 2b and 2c). In addition, since it is assumed that water vapor and CO_2 exchanges occur from only one side of the leaf, the boundary-layer resistance is doubled for water vapor ($2r_b$) and more than doubled for CO_2 ($2 \cdot 8r_b$). Evaporation from within the top soil layer
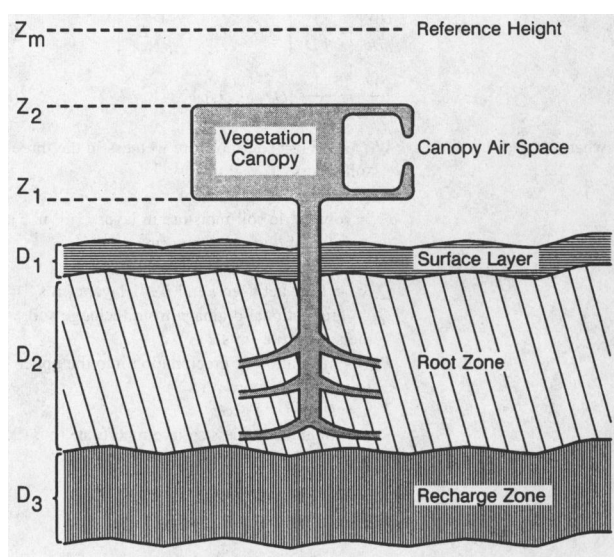
FIG. 1. Structure of the SiB2 model. SiB2 has only one vegetation layer, while SiB1 had provision for upper story and ground cover vegetation.
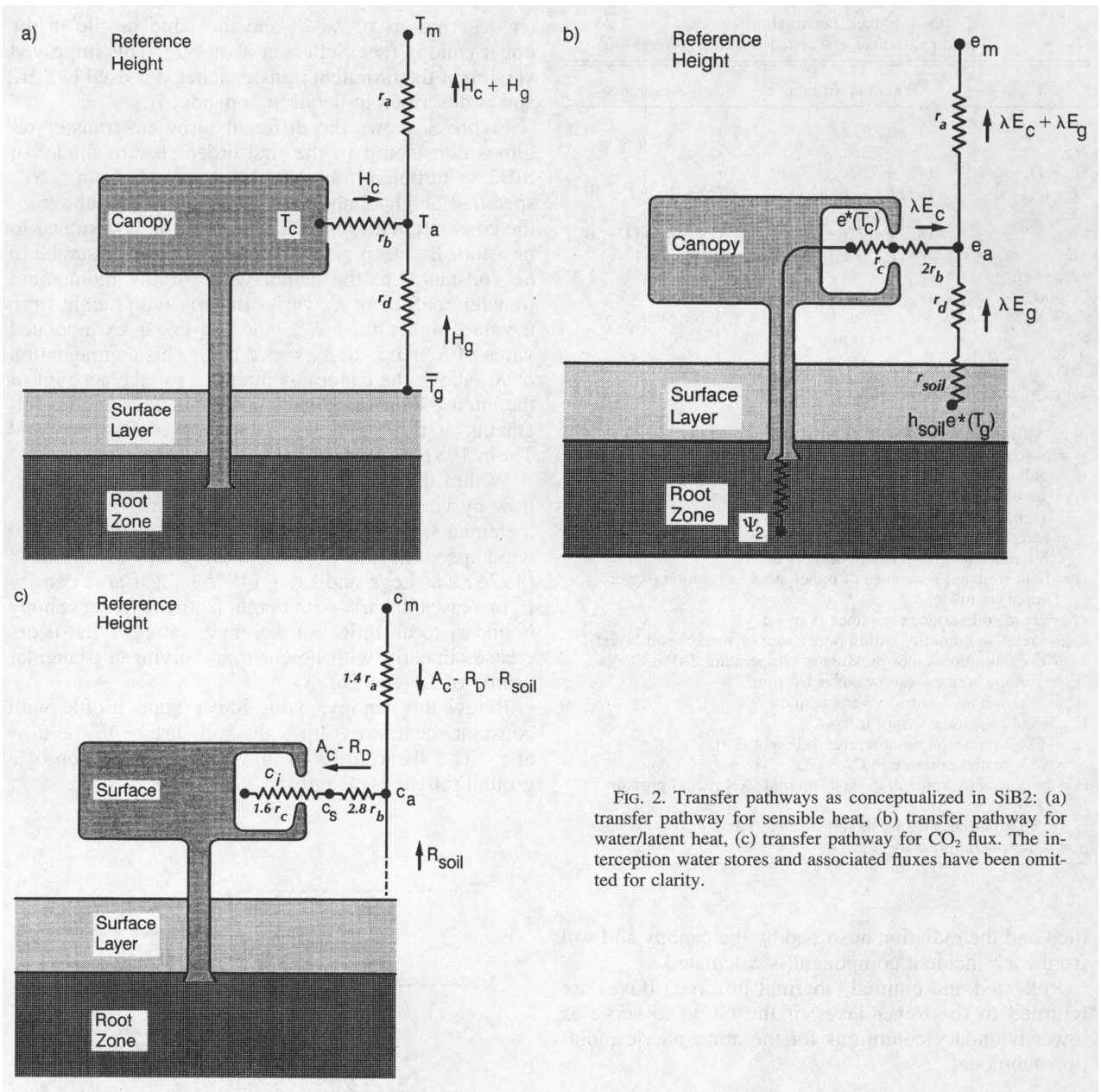
FIG. 2. Transfer pathways as conceptualized in SiB2: (a) transfer pathway for sensible heat, (b) transfer pathway for water/latent heat, (c) transfer pathway for CO_2 flux. The interception water stores and associated fluxes have been omitted for clarity.

E_{gs} must cross the soil surface resistance r_{soil}. Fluxes, potential differences, and resistances in Fig. 2 are summarized in Table 4.

Sections 5 through 9 of this paper review the calculations of radiative transfer; aerodynamic resistances; surface resistances and photosynthesis; soil hydrology; and the treatment of snow. Section 10 deals with the solution of the "fast" prognostic equations and time-stepping procedures.

5. Radiative transfer

The two-stream approximation model as described by Coakley and Chylek (1975) and Dickinson (1983) was extended by Sellers (1985) to describe the interception, reflection, transmission, and absorption of radiation by vegetation and soil. The fundamental equations were presented by Dickinson (1983) and are summarized in appendix A.

The radiation model used in SiB2 is only slightly modified from that of SiB1. Since SiB2 has one vegetation layer, only a single set of calculations for the canopy–soil system (one for each radiation component) need be performed each time step. Following the solution of the two-stream approximation model for the canopy–ground system (see Sellers 1985), the canopy reflectances, absorbances, and transmittances are spec-

TABLE 4. Fluxes, potential differences, and resistances associated with SiB2.

Flux	Potential difference	Resistance
H_c	$(T_c - T_a)\rho c_p$	r_b
H_g	$(T_g - T_a)\rho c_p$	r_d
$H_c + H_g$	$(T_a - T_m)\rho c_p$	r_a
λE_{ct}	$(e*(T_c) - e_a)\rho c_p/\gamma$	$(r_c + 2r_b)/(1 - W_c)$
λE_{ci}	$(e*(T_c) - e_a)\rho c_p/\gamma$	$2r_b/W_c$
λE_{gs}	$(h_{soil} e*(T_g) - e_a)\rho c_p/\gamma$	$(r_{soil} + r_d)/(1 - W_g)$
λE_{gi}	$(e*(T_g) - e_a)\rho c_p/\gamma$	r_d/W_g
$\lambda E_{ct} + \lambda E_{ci}$ $+ \lambda E_{gs} + \lambda E_{gi}$	$(e_a - e_m)\rho c_p/\gamma$	r_a
$A_c - R_D$	$(c_a - c_i)/p$	$1 \cdot 6\, r_c + 2 \cdot 8\, r_b$
R_{soil}	$(c_{soil} - c_a)/p$	$1 \cdot 4\, r_d$
$A_c - R_D - R_{soil}$	$(c_m - c_a)/p$	$1 \cdot 4\, r_a$

T_a, e_a = air temperature, vapor pressure in canopy air space (CAS) (K, Pa);
ρ, c_p = density, specific heat of air (kg m^{-3}, J kg^{-1} K^{-1});
γ = psychrometric constant (Pa K^{-1});
r_b = bulk canopy boundary layer resistance (sensible heat) (s m^{-1});
r_d = aerodynamic resistance between ground and canopy air space (sensible heat) (s m^{-1});
r_a = aerodynamic resistance between canopy air space and reference height (sensible heat) (s m^{-1})
r_c = bulk stomatal resistance of upper-story vegetation (water vapor) (s m^{-1});
r_{soil} = bare soil surface resistance (s m^{-1});
h_{soil} = relative humidity within pore space of surface soil layer;
$e*(T)$ = saturation vapor pressure at temperature T (Pa);
W_c = canopy wetness–snow cover fraction;
W_g = soil wetness–snow cover fraction;
R_{soil} = soil respiration (mol m^{-2} s^{-1});
c_m = CO_2 concentration at reference height (Pa);
c_a = CO_2 partial pressure in CAS (Pa);
c_i = bulk canopy value of c_i (leaf internal CO_2 partial pressure) (Pa);
c_{soil} = CO_2 partial pressure at soil surface (Pa);
p = atmospheric pressure (Pa).

ified and the radiation absorbed by the canopy and soil from each incident component is calculated.

Reflected and emitted (thermal infrared) fluxes are returned to the lower layer of the GCM to serve as lower boundary conditions for the atmospheric radiation submodel.

6. Aerodynamic resistances

The aerodynamic resistance model of SiB1 as documented in Sellers et al. (1986) described turbulent transfer processes above, within, and below a vegetation canopy of constant leaf-area density. This means that between the upper and lower bounds of the canopy (z_2 and z_1, respectively), the phytoelements were assumed to be uniformly distributed. This arrangement was found to give unrealistically large estimates of roughness length, z_0, when applied to a tropical forest case where the foliage was concentrated at the top of the canopy (see Shuttleworth et al. 1984), and so the scheme was modified to describe height-varying leaf-area densities (see Sellers et al. 1989). In this modified form, the first-order closure model provided much bet-

ter descriptions of z_0, d, and the wind profile in the upper canopy (see Sellers et al. 1989). This improved version of the turbulent transfer scheme is used in SiB2 and is described in detail in appendix B.

Figure 3 shows the different turbulent transfer regimes considered in the first-order closure model of SiB2. A turbulent transition layer extends from z_2 to a specified height z_t above the canopy. At and above z_t, the conventional log-linear wind profile is assumed to be valid. Between z_2 and z_t, shear stress is assumed to be constant, but the actual value of the momentum transfer coefficient K_m varies linearly with height from a value higher than K_m^* (the log-linear extrapolated value of K_m) at z_2 to $K_m = K_m^*$ at z_t. This augmentation of K_m above the canopy is intended to take account of the intense local turbulence generated by roughness elements at the top of the canopy (see Raupach and Thom 1981; Garratt 1978).

Within the canopy, shear is extracted from the airflow by viscous and bluff-body interactions with phytoelements, and K_m is made a linear function of local wind speed, in line with the observations of Denmead (1976) and Legg and Long (1975). Leaf area density L_d increases linearly with height from the lower canopy bound z_1 to an inflection height z_c, after which it decreases linearly with height to z_2, giving a triangular profile of L_d (see Fig. 3).

Below the canopy, a log-linear wind profile with constant shear stress links the soil surface to the flow at z_1. The shear stress in this layer is a function of a ground roughness length z_s.
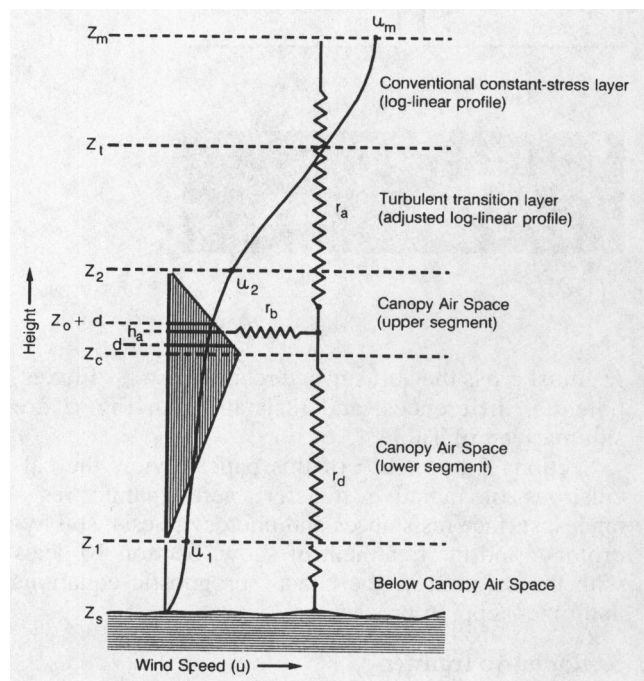

FIG. 3. Turbulent transfer regimes considered in the first-order closure model of SiB2.

The equations in appendix B yield profiles of u and K_m from above the canopy to the soil surface as functions of z_2, z_c, z_1, z_s, L_T, a leaf drag coefficient C_l, and two empirical parameters G_1 and G_4. These calculated profiles of u and K_m are then used to derive the aerodynamic resistance parameters used by SiB2.

The bulk canopy boundary-layer resistance (under neutral conditions) is given by

$$r_b = \frac{C_1}{(u_2)^{1/2}} = \left[\int_{z_1}^{z_2} \frac{L_d(u)^{1/2}}{p_s C_s} \, dz \right]^{-1}, \quad (10)$$

where

C_1 = bulk canopy boundary-layer resistance coefficient $(\text{m s}^{-1})^{-1/2}$;

u_2 = wind speed at z_2 (m s^{-1});

C_s = heat–mass transfer coefficient,
    $= 90(l_w)^{1/2}$,

l_w = leaf width (m);

p_s = leaf shelter factor (see appendix B).

The transfer coefficient for heat–mass transfer C_s is less than that for momentum C_l since C_l incorporates both bluff-body and viscous forces, while C_s describes only viscous transfer. The formulation of C_s is from Goudriaan (1977).

The ground to canopy air space (CAS) resistance r_d is defined as in SiB1 by

$$r_d = \frac{C_2}{u_2} = \int_{z_s}^{h_a} \frac{1}{K_s} \, dz, \quad (11)$$

where

C_2 = ground to CAS resistance coefficient;

K_s = heat–water vapor transfer coefficient, assumed to be equal to K_m $(\text{m}^2 \text{ s}^{-1})$;

h_a = canopy source height (m);

Canopy source height is assumed to be equal to the center of action of r_b within the canopy as obtained from the solution of

$$\int_{z_1}^{h_a} L_d(u)^{1/2} dz = \int_{h_a}^{z_1} L_d(u)^{1/2} dz. \quad (12)$$

Transfer between the CAS and the reference height, z_m, can be described exactly by piecewise integration of K_s ($= K_m$) over the distance from h_a to z_m, which includes within-canopy (h_a to z_2), turbulent transition layer (z_2 to z_t) and log-linear profile (z_t to z_m) segments:

$$r_a = \frac{C_3}{u_m} = \int_{h_a}^{z_m} \frac{1}{K_s} \, dz, \quad (13)$$

where

C_3 = aerodynamic (CAS to reference height) resistance coefficient.

In practice, within a GCM, the neutral value of C_3 is well approximated by the standard formulation for r_a:

$$C_3 \approx \left[\frac{1}{k} \log\left(\frac{z_m - d}{z_0} \right) \right]^2. \quad (14)$$

The coefficients C_1, C_2, and C_3 and the ratio $u_2 : u_m$ need only be calculated once for a given vegetation condition (type, geometry, LAI) to calculate r_a, r_b, and r_d under neutral conditions. The nonneutral adjustment to r_a is dependent on the GCM implementation [in off-line runs, a variation of the Paulson (1970) formulation is used], and simple changes are made to r_b and r_d such that

$$\frac{1}{r_b} = \frac{(u_2)^{1/2}}{C_1} + \frac{L_T}{890} \left(\frac{T_c - T_m}{l_w} \right)^{1/4} \quad (15)$$

$$\frac{1}{r_d} = \frac{u_2 \phi_H}{C_2}; \quad \phi_H \geq 1$$

$$\phi_H = \left[1 + 9 \frac{(T_g - T_m)}{T_g u_2^2} z_2 \right]^{1/2}. \quad (16)$$

Derivations of (15) and (16) may be found in the appendix of Sellers et al. (1986).

The aerodynamic parameters C_1, C_2, and C_3 (z_0 and d) are thus calculated as functions of (i) the empirical constants G_1 and G_4, which were obtained from curve-fits to second-order closure model results; (ii) time in-variant vegetation-type-dependent properties z, z_2, z_c, z_1, z_s, and C_l (l_w, l_L, χ_L); and (iii) a time-varying, vegetation-type-dependent parameter, the total LAI, L_T. It is impractical to calculate C_1, C_2, z_0, and d at every time step or even whenever the LAI is incremented. [In the GCM run described in Randall et al. (1995), L_T is changed daily at every grid square.] Instead, the calculation of these parameters is performed off-line for each vegetation type for L_T values ranging from zero to 8.0 at $0.5 L_T$ intervals by a program called AERSET. The resulting $12 \times 17 \times 4$ table AEROSIB (12 vegetation types $\times 17 L_T$ values $\times 4$ parameters: C_1, C_2, Z_0, d) is accessed by the SiB2 preprocessor MAPPER, which also has access to monthly values of L_T supplied by satellite data and a vegetation-type map, to specify monthly global fields of C_1, C_2, z_0, and d by linear interpolation between the AEROSIB L_T values (see Sellers et al. 1995). Within the GCM, daily interpolated values of these parameters, adjusted for snow cover effects (see section 9), are used to calculate time step values of r_b, r_d, and r_a using (15), (16), and a GCM-dependent variation of (14), respectively. The variables required from SiB2-GCM at each time step are u_m (from which u_2 is estimated as a ratio), T_c, T_g, T_a, and T_m. Where r_a is dependent on virtual temperature, e_a and e_m are also required.

The model described above is physically naive. In particular, it is very doubtful that a first-order closure model of this type can describe transfer processes below a vegetation canopy in a credible way (see Shaw and Pereira 1982). However, the model does seem to reproduce the gross dependencies of z_0 and d on in-

creasing LAI, as well as provide an acceptable description of momentum transfer above tall vegetation (see Sellers et al. 1989).

7. Surface resistances and canopy photosynthesis

a. Canopy transpiration and photosynthesis

In SiB1, the stomatal resistance (conductance) of individual leaves, r_s ($=1/g_s$), was described by the empirical model of Jarvis (1976), which required the use of a large number of vegetation-type-dependent parameters, many of which are hard to specify from the ecological literature (see Sellers et al. 1986; Dorman and Sellers 1989; Sellers et al. 1989). Photosynthesis was not addressed in SiB1.

The C_3 photosynthesis model of Farquhar et al. (1980), as expanded on by Collatz et al. (1991) and others, the C_4 model of Collatz et al. (1992), and the stomatal model of Ball (1988) are the basis for the leaf photosynthesis–conductance model used in SiB2. In this model, photosynthesis and conductance are explicitly connected (see Fig. 4). A complete description of the model is reproduced in appendix C; a summary of the approach is given below.

The Collatz et al. (1991) version of the model for C_3 species describes the leaf assimilation (or gross photosynthetic) rate as the minimum of three limiting rates, w_c, w_e, w_s, where w_c, w_e, and w_s are functions that describe the assimilation rates as limited by the efficiency of the photosynthetic enzyme system (Rubisco-limited), the amount of PAR captured by the leaf chlorophyll, and the capacity of the leaf to export or utilize the products of photosynthesis, respectively. For C_4 species, the terms w_c and w_e still refer to Rubisco and light limitations, respectively, but w_s now refers to a PEP-Carboxylase limitation (see Collatz et al. 1992). Thus,

$$A \leqslant \text{Min}(w_c, w_e, w_s), \qquad (17)$$

where

A = leaf photosynthetic rate (mol m^{-2} s^{-1});
w_c = Rubisco (leaf enzyme) limited rate of assimilation (mol m^{-2} s^{-1});
w_e = light-limited rate of assimilation (mol m^{-2} s^{-1});
w_s = Carbon compound export limitation (C_3 vegetation), or PEP-Carboxylase (C_4) limitation on photosynthesis (mol m^{-2} s^{-1}).

The physiological limit on assimilation w_c is primarily a function of the leaf's enzyme reserves, which can be thought of as the biochemical processing capacity of the leaf. This capacity is represented in the model by a parameter V_{max}, the maximum catalytic capacity of the photosynthetic enzyme, Rubisco, multiplied by a temperature-dependent function and a soil moisture stress function (see appendix C). Thus, w_c can be written as

$$w_c = f_c(V_{max}, T_c, W_2, c_i, O_2, \cdots), \qquad (18)$$
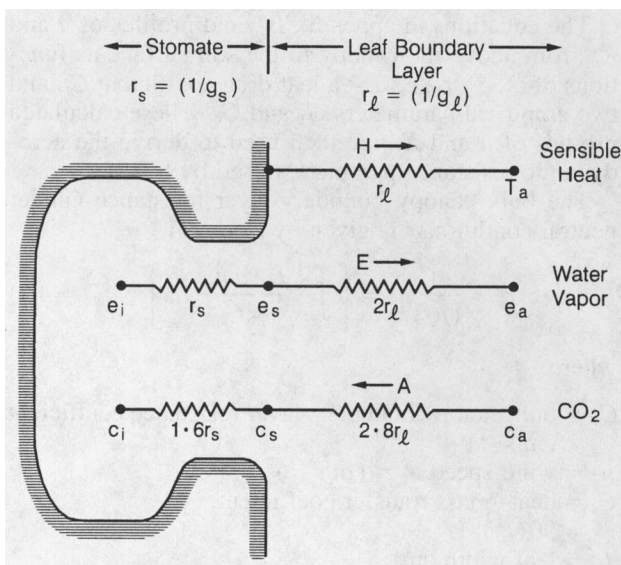
FIG. 4. Coupled leaf stomatal photosynthesis–conductance models as described by Collatz et al. (1991). System shows pathways for heat, CO_2, and water vapor flux (reproduced from Sellers et al. 1992a). Term r_l refers to the two-sided leaf laminar boundary-layer resistance for sensible heat: water and CO_2 are assumed to be lost from one side of the leaf only; r_b is the canopy integral of r_l; and r_c is the canopy integral of r_s.

where

c_i = partial pressure of CO_2 in leaf interior (Pa);
O_2 = partial pressure of O_2 in leaf interior (Pa).

The light-limited rate of assimilation is defined by

$$w_e = f_e(\epsilon \mathbf{F}_\pi \cdot \mathbf{n}, c_i, O_2, \cdots), \qquad (19)$$

where

$\mathbf{F}_\pi$ = (vector) flux of PAR incident on leaf (W m^{-2});
$\mathbf{n}$ = leaf normal;
ϵ = quantum efficiency for CO_2 uptake (mol mol^{-1} or mol J^{-1}).

The storage–export limiting rate on assimilation is given by

$$w_s = f_s(V_{max}, T_c, W_2). \qquad (20)$$

Leaf net assimilation is given by subtracting the leaf maintenance respiration rate from A, itself a function of the leaf's enzyme pool size as represented by V_{max}:

$$A_n = A - R_d = A - f_r(V_{max}, T_c, W_2, \cdots), \qquad (21)$$

where

A_n = net assimilation rate (mol m^{-2} s^{-1});
R_d = leaf respiration rate (mol m^{-2} s^{-1}).

The complete forms for the functions f_c, f_e, f_s, and f_r may be found in appendix C.

Collatz et al. (1991) went on to combine this photosynthetic model with the Ball (1988) semiempirical model for leaf stomatal conductance:

$$g_s = m \frac{A_n}{c_s} h_s p + b, \qquad (22)$$

where

g_s = leaf stomatal conductance (mol m^{-2} s^{-1});
m = empirical coefficient from observations,
$\quad$ = 9 for C$_3$ vegetation,
$\quad$ = 4 for C$_4$ vegetation,
$\quad$ = 6 for conifers;
b = empirical coefficient from observations (mol m^{-2} s^{-1}, or m s^{-1}),
$\quad$ = 0.01 for C$_3$ vegetation,
$\quad$ = 0.04 for C$_3$ vegetation;
h_s = relative humidity at leaf surface;
c_s = CO$_2$ partial pressure at leaf surface (Pa);
p = atmospheric pressure (Pa).

In (22), leaf conductance for the influx of CO$_2$ and the simultaneous efflux of water are directly linked through a simple dependence on relative humidity, CO$_2$ concentration, and two vegetation-dependent constants m and b. This represents a considerable simplification over the more empirical model of leaf conductance used in SiB1 that required the definition of many species-specific parameters.

In (17) through (22), the partial pressures of CO$_2(c_i, c_s)$ and the leaf-surface relative humidity h_s are linked to conditions in the canopy air space via the leaf stomatal conductance g_s; the leaf boundary-layer conductance g_l; the net flux of CO$_2$ A_n; and leaf transpiration E_{lt} (see Fig. 4 and appendix C). The equations describing these fluxes allow us to close the set (17) through (22) and thus calculate mutually consistent values of A_n and E_{lt} for steady-state conditions. Sellers et al. (1992a) describe an interative procedure for doing this, which is used in the off-line version of SiB2. In the GCM version of SiB2, we use a more efficient method based on a prognostic equation for leaf or canopy conductance (see appendix C).

The equation set reviewed above is relevant to a single leaf with known physiology ($V_{max}, \epsilon, m, \ldots$), physical properties, and forcing conditions ($T_c, F_\pi, e_a, u, W_2, c_a$). The next step is to integrate these equations over the depth of the canopy to describe canopy photosynthesis A_c and conductance g_c. Sellers et al. (1992a) describe a procedure for doing this, which is based on the hypothesis that the canopy depth-profile of leaf nitrogen, and hence V_{max}, follows the time-mean (radiation-weighted) profile of PAR:

$$V_{max_L} = V_{max_0} e^{-\bar{k}L}, \qquad (23)$$

where

V_{max_0}, V_{max_L} = values of leaf V_{max} at the top of the canopy, (0), and under a LAI L, respectively (mol m^{-2} s^{-1});
$\bar{k}$ = time-mean (radiation-weighted) extinction coefficient for PAR.

The amount of PAR incident on an average leaf surface within the canopy, $\mathbf{F}_\pi \cdot \mathbf{n}$, can be approximated by

$$\mathbf{F}_\pi \cdot \mathbf{n} \approx F_{\pi_0} \left[\frac{G(\mu)}{\mu} \right] e^{-\bar{k}L}, \qquad (24)$$

where

F_{π_0} = incident PAR flux (W m^{-2});
$G(\mu)$ = projection of leaves in direction of incoming radiation flux (μ).

The use of a time-mean value of $\bar{k}$ in (24) instead of the more correct instantaneous value of k gives rise to only small errors in the estimation of w_e (see Sellers et al. 1992a). The total incident PAR flux, F_{π_0}, is estimated by summing the incident direct beam and diffuse visible fluxes, $F_{\pi_0} \approx F_{v,b_0}, + F_{v,d_0}$. Since w_c, w_e, and w_s now have the same depth-profile relationships through $e^{-\bar{k}L}$, we may substitute (23) into (18) and (20), and substitute (24) into (19), then integrate to give us an expression for canopy photosynthesis, A_c.

So far, we have only considered the case of a continuous, green canopy as described in Sellers et al. (1992a), where the canopy-cover fraction V is unity. This analysis can be adapted to cover the case of clumped vegetation ($V < 1$) containing some nongreen phytoelements ($N < 1$). In the case of clumped vegetation, the local LAI, that is, the LAI within the clumps, is given by L_T/V.

Thus, if we retain the physiological parameters for the top leaves as being representative of green leaves only (V_{max_0}), we can write

$$A_c = A_{n_0} \int_0^{L_T/V} V N e^{-\bar{k}L} dL = A_{n_0} \Pi, \qquad (25)$$

where

$A_{n_0} = A_n$ for leaves at the top of the canopy (mol m^{-2} s^{-1}),
$\quad = f_c(V_{max_0}, \cdots), f_e(F_{\pi_0}, \cdots), f_s(V_{max_0}, \cdots)$;

$$\Pi = \frac{VN(1 - e^{-\bar{k}L_T/V})}{\bar{k}};$$

$$\Pi \approx \text{FPAR}/\bar{k}.$$

This value of A_c can then be used to calculate a consistent canopy conductance g_c by adapting (22):

$$g_c = m \frac{A_c}{c_S} h_S p + bL_T, \qquad (26)$$

where the larger "S" subscript refers to bulk canopy values of c_s and h_s. This value of g_c is used to calculate the canopy transpiration rate E_{ct} by

$$\lambda E_{ct} = \left[\frac{e*(T_c) - e_a}{1/g_c + 2r_b} \right] \frac{\rho c_p}{\gamma} (1 - W_c), \qquad (27)$$

where

$e^*(T_c)$ = saturated vapor pressure at temperature T_c (Pa);

e_a = canopy air space vapor pressure (Pa);

ρ, c_p = density, specific heat of air, respectively (kg m^{-2}, J kg^{-1} K^{-1});

γ = psychrometric constant (Pa K^{-1});

W_c = fractional wetted area of the canopy.

The complete set of leaf-scale and canopy-integrated equations governing photosynthesis and conductance is written out in appendix C but can be summarized as follows:

$$\begin{bmatrix} \text{canopy} \\ \text{biophysical} \\ \text{rate variable} \end{bmatrix} = \begin{bmatrix} \text{leaf physiology} \\ \text{or radiation rate} \\ \text{limit (top leaves)} \end{bmatrix}\begin{bmatrix} \text{environmental} \\ \text{forcing or} \\ \text{feedback terms} \end{bmatrix}\begin{bmatrix} \text{canopy} \\ \text{PAR-use} \\ \text{parameter} \end{bmatrix}. \tag{28}$$

$$A_c, g_c \quad = \quad [V_{\text{max}_0}, F_0] \quad\quad [B_1 \cdots B_6] \quad\quad [\Pi]$$

In (28), the roles of the top leaf performance and the canopy PAR-use parameter Π can be seen clearly. Here Π varies between zero for no vegetation cover, to between 1 and 1.5 for dense green vegetation. The parameters B_1 through B_6 are defined in appendix C; they describe the effects of temperature, humidity, CO_2 concentration, soil moisture stress, etc., on A_c and g_c. Note that the near-surface atmospheric CO_2 concentration c_m has an indirect effect on A_c and g_c through the CO_2 flux pathway and hence c_i and c_s (see Figs. 2 and 4).

Term Π is the critical variable that can be obtained from satellite data. Discussion in Sellers et al. (1992a) shows how the FPAR term in Π is near-linearly related to the simple ratio vegetation index when the soil background is dark:

$$\text{FPAR} \propto \text{SR} = \frac{a_N}{a_V}, \tag{29}$$

where

SR = simple ratio vegetation index;

a_N, a_V = near-infrared, visible reflectances or counts, respectively (sensor-dependent).

The approximate scale-invariance of (29) is key to its application on large spatial scales, such as in a GCM. Comparing (28) and (29), we see that there is a chain of (near-) linear relationships between A_c, g_c, Π, FPAR, and SR. Since the area-integral of a linear function is directly proportional to the average of that function over the domain, it can be demonstrated that the mean value of SR over a large area, as supplied by a coarse-resolution satellite sensor, should provide good estimates of A_c and g_c over the same area through Π in (28) (see Sellers et al. 1992a, 1996). This effect was explored using field data from the FIFE experiment (see Sellers et al. (1992c), where it was shown that the scheme was robust over a wide range of length scales and conditions.

The methods for converting the raw satellite data into estimates of FPAR, L_T, and N are discussed in full in Sellers et al. (1996).

b. Precipitation interception and interception loss

There are two important features in the treatment of precipitation interception and interception loss in SiB2.

(i) The hydrological effects resulting from the spatial nonuniformity of convective precipitation are explicitly addressed.

(ii) The canopy and ground are each assigned separate liquid water and snow–ice interception stores: M_{cw} and M_{cs} for the canopy and M_{gw} and M_{gs} for the ground. If both phases of water coexist on either surface at the end of a time step, the liquid water store (subscript "w") is lost to drainage, runoff, or infiltration into the soil, leaving only the snow–ice component "s" in place. The ground snow store M_{gs} covers a variable fraction of the surface at low values and can maintain a different temperature from the exposed soil surface. All phase changes, whether due to energy inputs or interception of precipitation of a different surface temperature from the stored water already in place, are taken into account.

These features are reviewed briefly below; details can be found in appendix D.

A full description of the convective precipitation interception formulation is given in Sato et al. (1989b). In SiB2, the possibilities of convective snowfall and of convective rainfall falling on snow-covered areas are excluded for simplicity; thus, only liquid convective precipitation falling on surfaces above freezing is permitted in the model. In nature, the net effect of the "clumped" precipitation patterns typical of convective storms is to increase the area-averaged canopy throughfall and surface (infiltration excess) runoff rates. In most GCMs, a single (area averaged) figure for convective precipitation is produced for each grid area for each time step.

In SiB2, we assume that convective rainfall is spatially distributed according to a simple exponential function I_{cx} (see Fig. 5). The coefficients in this function can also be adjusted to represent large-scale (spatially uniform) precipitation I_{l_x}. Since most models can produce both types of precipitation simultaneously,
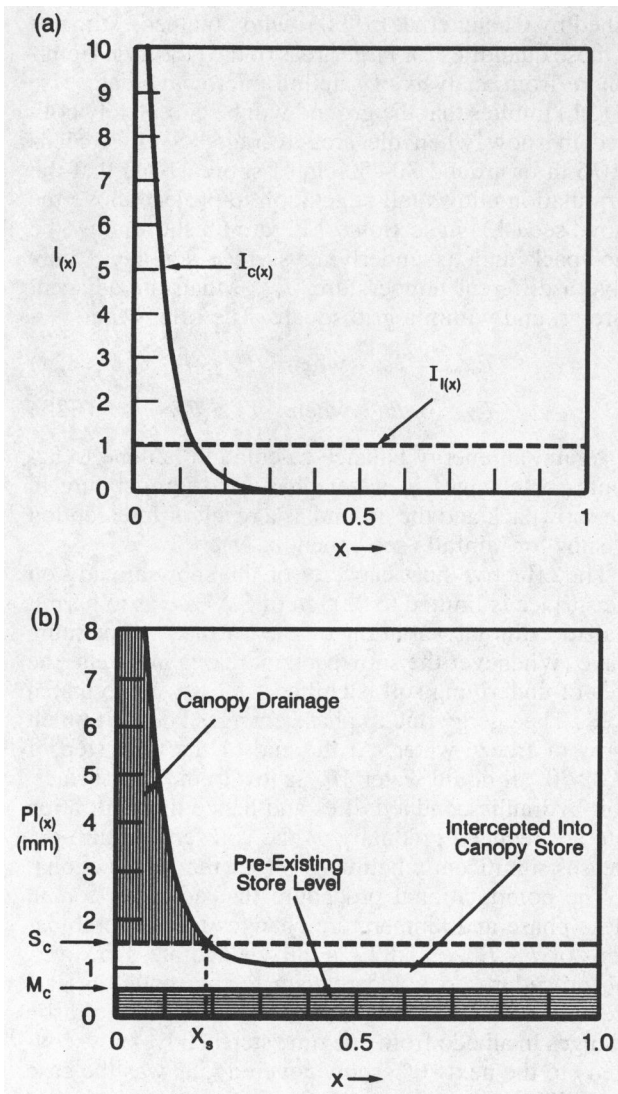
(a)

(b)

FIG. 5. (a) Precipitation area–amount relationships used in SiB2. The variable x refers to fraction of the grid area, the variable $I_{(x)}$ refers to the relative amount of precipitation. Note that the large-scale precipitation $I_{l(x)}$ is almost invariant over the grid area, while convective precipitation $I_{c(x)}$ is nonuniformly distributed. (b) Dynamics of precipitation interception by a vegetation canopy in SiB2. The amount of water already stored in the canopy prior to rainfall interception, $M_{cs} + M_{cw}$, is considered to be uniformly distributed over the grid area (see horizontally hatched area). The integral of the water amount above $M_{cs} + M_{cw}$ represents the total amount of water intercepted by the canopy. Here x_s is the proportion of the grid area where the intercepted rainfall plus the preexisting canopy water storage, $M_{cs} + M_{cw}$, exceeds the canopy storage limit S_c. All water above the S_c limit drains off the canopy to form D_c (vertically hatched area), all below it is added to the canopy interception store.

their contributions to the total rainfall rate can be combined into a single area–amount function by weighting these coefficients to give a precipitation rate as a function of fractional area $PI_{(x)}$ where $P = P_c + P_l$.

The direct throughfall component, that is, the rainfall that falls through the gaps in the canopy, is calculated

by a modification of the radiative transfer model. This leaves us with the rainfall that is intercepted but not necessarily retained by the canopy. The next step is to calculate the proportion of the grid area for which the canopy has intercepted enough rainfall to equal or exceed its saturation limit. This proportion x_s is shown schematically in Fig. 5 and is given by the solution to

$$PI_{(xs)} = S_c - M_{cs} - M_{cg}, \qquad (30)$$

where

$S_c = $ canopy storage limit (m),
$\quad = 0.0001 L_T$.

Figure 5b shows how the precipitation area-amount function is added to the water or snow already stored on the canopy, M_{cw} or M_{cs}, respectively, which is assumed to be uniformly distributed at the beginning of the time step, and how x_s relates to S_c. The equation set may be integrated to provide an estimate of the canopy drainage loss that is equivalent to the vertically hatched area in Fig. 5b. This water joins the throughfall to provide an effective precipitation rate for the ground surface. A similar calculation to (30) is done for the surface "puddle" storage, which has a maximum value of 0.2 mm for M_{gw}.

The residual precipitation rate reaching the ground surface can still exceed the local infiltration capacity of the soil. For the sake of simplicity, we assume the same area–amount relationship for this ground surface rainfall rate, which in fact would have been distorted by interception in the canopy, etc. Overland flow is generated for the fraction of the grid area where this residual rainfall rate exceeds the local soil hydraulic conductivity.

Once the precipitation has been intercepted by the canopy or ground, some calculations must be made to take account of possible phase changes. The canopy moisture stores M_{cw} or M_{cs} and the canopy itself are at a specified temperature T_c prior to the interception of precipitation at temperature T_m. A simple energy balance calculation is performed to calculate a single new temperature for the canopy, the intercepted precipitation, and the frozen or melted water produced as a result of phase changes (see appendix D). At the end of the calculation, if M_{cs} and M_{cw} are both positive, M_{cw} is lost and added directly to the soil moisture store W_1. This prohibits the retention of two different phases of water that would make for complications at the next time step.

A similar procedure is used to account for temperature and phase changes on the ground. However, SiB2 incorporates a treatment of nonuniform snow cover that must be factored into the calculation. Figure 6a shows how snow extent varies linearly with snow water equivalent according to

$$A_s = a_s M_{gs}, \qquad (31)$$
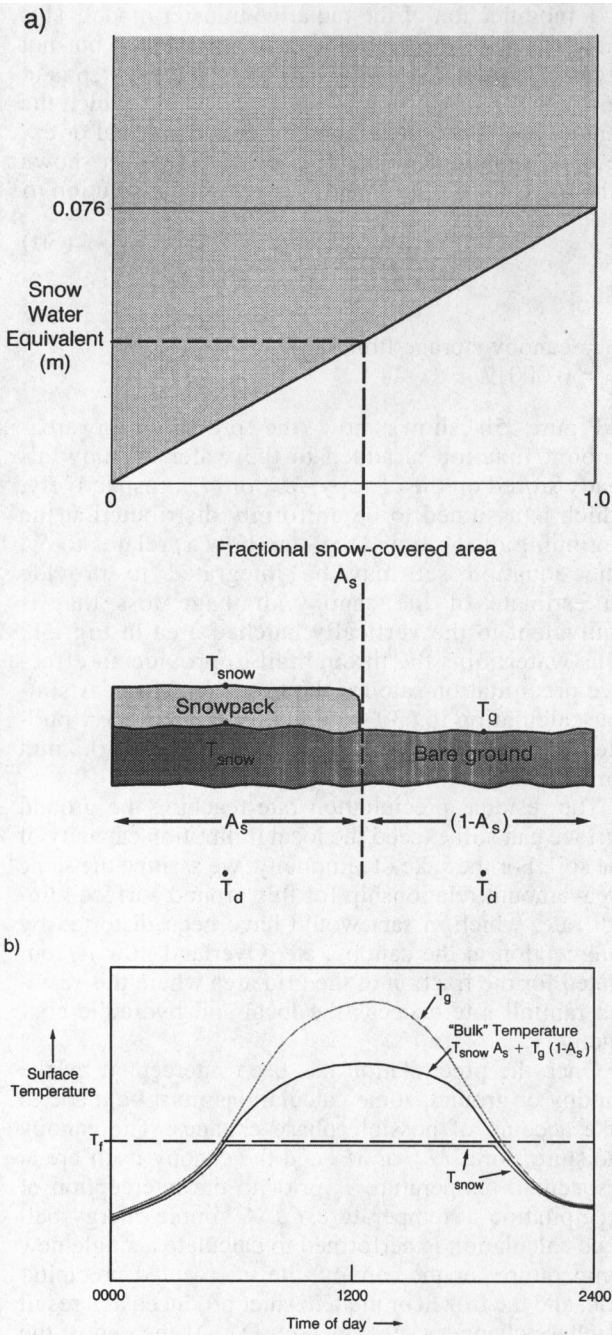
FIG. 6. (a) Relationship between SWE and snow extent over a grid area as modeled in SiB2, based on data published by Chang et al. (1990). (b) Diurnal cycle of ground and snowpack temperature for a patchy snow cover as represented by SiB2. Note that the combined effective temperature, $T_B = T_{snow}A_s + T_g(1 - A_s)$, is used for aerodynamic and radiation exchange calculations.

where

A_s = snow-covered area, $0 \leqslant A_s \leqslant 1$,
$a_s = 13.2$ (m^{-1}).

The value of a_s was determined from snow water equivalent (SWE) and snow cover extent data pub-

lished by Chang et al. (1990), who obtained estimates of these quantities for large areas of the Northern Hemisphere from analysis of satellite microwave data. Use of (31) implies that the ground will be completely covered in snow when the area-averaged SWE exceeds 0.076 m or around 30–50 cm of snow. [Note that the formulation allows tall vegetation to project above the snow, see (42) in section 9.] Figure 6b shows how the snowpack and its underlying surface soil layer may have a different temperature, T_{snow}, than the adjacent bare ground within a grid square. The rule is that

$$T_{snow} = T_g, \quad \text{when} \quad T_g < T_f \qquad (32a)$$

$$T_{snow} = T_f, \quad \text{when} \quad T_g > T_f. \qquad (32b)$$

Again, an energy balance calculation is done to account for changes in water phase and temperature in the snowpack and the ground as a result of interception of snow or rainfall (see appendix D).

The effective heat capacity of the snow already on the surface is limited to 0.05 m of SWE so as to permit realistic diurnal variation of the surface temperature wave. Whenever the snowpack increases in extent, the area of underlying soil is chilled (if $T_g > T_f$) to match T_{snow}. The energy due to phase changes is used to melt snow or freeze water. At the end of the time step, if $M_{gs} > 0$, all liquid water M_{gw} is lost to the soil surface. Soil hydraulic conductivities and hence the infiltration rate are reduced gradually as the soil temperature decreases significantly below zero (see the next section).

The computational procedure that accounts for all these phase and temperature changes for all combinations of T_g, T_{snow}, and T_m is fairly elaborate. However, the procedure does add realism to the model as grid areas with thawing snow do not undergo any drastic changes in albedo from one time step (100% snow covered) to the next (0% snow covered), as was the case for SiB1. Instead, the transition in snow cover and hence albedo takes place over several days. Likewise, the bulk ground surface temperature, represented as $T_B = T_{snow}A_s + T_g(1 - A_s)$, undergoes a similar gradual transition.

From then on, interception loss is treated in SiB2 in a similar way as in SiB1:

$$\lambda E_{ci} = \left[\frac{e*(T_c) - e_a}{r_b} \right] \frac{\rho c_p}{\gamma} W_c \epsilon_{T_c}, \qquad (33a)$$

$$\lambda E_{gi} = \left[\frac{e*(T_x) - e_a}{r_d} \right] \frac{\rho c_p}{\gamma} W_g \epsilon_{T_g}, \qquad (33b)$$

where

$W_c = (M_{cw} + M_{cs})/S_c, \ 0 \leqslant W_c \leqslant 1;$
$W_g = M_{gw}/0.0002$ or $A_s;$
$T_x = T_{snow}$ if $M_{gs} > 0,$
$\quad = T_g$ if $M_{gw} > 0;$
$\epsilon_{Tc,g} = 1$ when $M_{c,gw} > 0,$
$\quad = \lambda/(\lambda + \lambda_s),$ when $M_{c,gs} > 0;$
$\lambda_s =$ heat of sublimation (J kg^{-1}).

The interception losses and/or condensation gains calculated from (33) are factored into (1) through (5) during the time-stepping procedure. Some adjustments are made to canopy and ground radiative and aerodynamic properties whenever M_{cs} or M_{gs} are nonzero (see section 9).

c. Soil evaporation

Evaporation of soil moisture from within the top soil layer in SiB2 is calculated by

$$\lambda E_{gs} = \left[\frac{[h_{soil}e^*(T_g) - e_a]}{r_{soil} + r_d} \right] \frac{\rho c_p}{\gamma} (1 - W_g), \quad (34)$$

where

r_{soil} = soil surface resistance (s m^{-1});
h_{soil} = relative humidity of the soil pore space;
  $= \exp(\psi_1 g / RT_g)$, when $e^*(T_g) \geqslant e_a$,
  $= 1$, when $e^*(T_g) < e_a$;
ψ_1 = soil moisture potential of top layer (m);
g = acceleration due to gravity (m s^{-2});
R = gas constant (J kg^{-1} K^{-1}).

The soil resistance term, r_{soil}, is an empirical term that is supposed to take into account the impedance of the soil pores to exchanges of water vapor between the bulk of soil layer 1 and the immediately overlying air. Sun (1982), followed by Camillo and Gurney (1986), Villalobos and Fereres (1990), and Sellers et al. (1992c), all found it necessary to include this term to prevent the simulation of excessive soil evaporation rates. We will use (19) of Sellers et al. (1992c), which was derived from analyses of a large number of surface flux observations in FIFE:

$$r_{soil} = \exp(8.206 - 4.255W_1). \quad (35a)$$

However, in the work discussed in Randall et al. (1996), we use a functionally similar expression fitted to the same data:

$$r_{soil} = \text{Max}(23.6, 694 - 1500W_1). \quad (35b)$$

Further discussion of the physical mechanisms involved and other field studies on r_{soil} may be found in Sellers et al. (1992c).

8. Diffusion of water and heat in the soil

A three-layer isothermal model was used in SiB1 to calculate the hydraulic diffusion and gravitational drainage of water in the soil. The equation used to describe vertical exchanges between soil layers is

$$Q = K \left[\frac{\partial \psi}{\partial z} + 1 \right], \quad (36)$$

where

Q = vertical water flow (m s^{-1});
K = hydraulic conductivity (m s^{-1}),
  $= K_s W^{(2B+3)}$;

ψ = soil moisture potential (m),
  $= \psi_s W^{-B}$;
$K_s, \psi_s = K, \psi$ at saturation (m s^{-1}, m);
B = empirical parameter.

In (36), the term "+1" accounts for gravitational drainage.

The drainage of water out of the bottom of the soil column to create base flow is given by

$$Q_3 = f_{ice}\left(\sin\varnothing_s K_s W_3^{(2B+3)} + 0.001 \frac{\theta_s D_3 W_3}{\tau_d} \right), \quad (37)$$

where

$\varnothing_s$ = local slope angle.

The first term in the parentheses on the right-hand side of (37) covers gravitational drainage as modeled in SiB1. The second term was proposed by Liston (1992, personal communication) to account for the contributions to base flow made by heterogeneities in the soil moisture fields of large river basins. The factor f_{ice} allows for a progressive reduction in soil hydraulic conductivity as the soil freezes; it is defined below in (38).

The solution of (6), (7), (8), (36), and (37) is accomplished using an improved backward-implicit scheme operating on the final (end of time step) values of Q holding between two soil layers; that is, on ($Q + \Delta Q)_{i,i+1}$. Estimates of the time-averaged soil conductivity, $\bar{K}_{i,i+1}$, holding between two layers for the same period are derived following the methods of Milly and Eagleson (1982), whereby

$$\bar{K}_{i,i+1} = f_{ice}\left[\frac{K_i\psi_i - K_{i+1}\psi_{i+1}}{\psi_{i+1} - \psi_i} \right]\left[\frac{B}{B+3} \right], \quad (38)$$

where

$f_{ice} = (T_x - (T_f - 10))/10; 0.05 < f_{ice} \leqslant 10$,
$T_x = T_g$ for $\bar{K}_{1,2}$,
  $= T_d$ for $\bar{K}_{2,3}$ or Q_3.

The values of $\bar{K}$ estimated at the beginning of a time step are bounded by the minimum value of K_i found within the profile (lower bound) and the value of $\bar{K}_{i,i+1}$ that would be obtained at the end of the time step assuming free gravitational drainage (upper bound).

Heat transport in the soil is described by the force–restore model of Deardorff (1977) [see (2) and (3)]. The heat capacity of the diurnally responsive upper soil, C_g, is defined after the work of Camillo and Schmugge (1981), who formulated expressions for soil thermal conductivity and specific heat as functions of porosity and soil moisture content. We have added a term to take some account of the thermal effects of snow (see appendix E).

9. Effects of snow on surface reflectance and aerodynamic properties

The formulation of snow interception in SiB2 is described in section 7 and appendix D. The buildup of

snow on the canopy and ground affects surface reflectance and aerodynamic properties.

The reflectance and transmittance of canopy elements as used in the radiative transfer submodel are altered as follows:

$$\bar{\rho}_\Lambda = (1 - W_{cs})\rho_\Lambda + W_{cs}\rho_{\text{snow}_\Lambda} \qquad (39a)$$

$$\bar{\delta}_\Lambda = (1 - W_{cs})\delta_\Lambda + W_{cs}\delta_{\text{snow}}\delta_\Lambda, \qquad (39b)$$

where

$\bar{\rho}_\Lambda$ = altered reflectance of canopy phytoelement in wavelength interval Λ;

ρ_Λ = snow-free value of phytoelement reflectance in wavelength interval Λ;

$\bar{\delta}_\Lambda, \delta_\Lambda$ = same as $\bar{\rho}_\Lambda, \rho_\Lambda$, except for phytoelement transmittance;

W_{cs} = snow-covered fraction of canopy,
    = $0.5 M_{cs}/S_c$, $(0 \leqslant W_{cs} \leqslant 0.5)$;

$\rho_{\text{snow}_\Lambda}$ = reflectance of snow-covered part of canopy;

$\delta_{\text{snow}_\Lambda}$ = transmittance of thin snow layer.

Snow reflectance is reduced by around 60% as the snow melts and snow transmittance increases in more or less the same way (Chang 1990, personal communication). We therefore use

$$\rho_{\text{snow}_V} = 0.8 f_{\text{melt}}; \quad \rho_{\text{snow}_N} = 0.4 f_{\text{melt}} \qquad (40a)$$

$$\delta_{\text{snow}_V} = 1 - 0.8 f_{\text{melt}}; \quad \delta_{\text{snow}_N} = 1 - 0.46 f_{\text{melt}} \qquad (40b)$$

$$f_{\text{melt}} = 1 - 0.04(T_g - T_f); \quad 0.6 \leqslant f_{\text{melt}} \leqslant 1.$$

The ground reflectance is dealt with in a similar way

$$\bar{\rho}_{\text{soil}_\Lambda} = \rho_{\text{soil}_\Lambda}(1 - A_s) + A_s\rho_{\text{snow}_\Lambda}. \qquad (41)$$

All surfaces, whether snow covered or not, are assumed to have emissivities and absorbances of unity in the thermal infrared ($\Lambda = T$).

The aerodynamic properties of SiB2 are altered very simply as the ground snowpack M_{gs} accumulates. The proportion of canopy that is exposed above the snowpack, Z, is used to adjust the values of d, z_0, C_1, and C_2 as defined in section 6. Here Z is calculated by assuming that the snowdepth is five times the snow-water equivalent:

$$Z = 1 - \left[\frac{5M_{gs} - z_1}{z_2 - z_1}\right], \quad 0.1 < Z \leqslant 1.0 \qquad (42a)$$

$$\bar{d} = z_2 - Z(z_2 - d) \qquad (42b)$$

$$\bar{z}_0 = z_0 \frac{(z_2 - \bar{d})}{(z_2 - d)} \qquad (42c)$$

$$\bar{C}_1 = C_1/Z \qquad (42d)$$

$$\bar{C}_2 = C_2 Z. \qquad (42e)$$

In (42), an overbar denotes the altered quantity used in on-line calculations.

10. Solution of the equation set

The sequence of calculations carried out by SiB2 as implemented in the Colorado State University GCM is set out in Fig. 7 and is summarized below.

The time-invariant boundary conditions for each grid square are continuously available (see Table 1). The time-varying vegetation parameters (FPAR, L_T, N, $\bar{k}$, z_0, d, C_1, and C_2) that are all dependent on the spectral vegetation indices provided by satellite data are interpolated daily from a set of monthly values [see Sellers et al. (1996) and the "OFF-LINE" procedures in Fig. 7]. A single pass through the model proceeds as follows:

(i) The values of the prognostic variables T_c, T_g, T_d, M_c, and M_g are used to adjust time-invariant aerodynamic properties of the surface using (42).

(ii) The radiative transfer model is used to calculate the absorption and reflection of radiation by canopy and ground. First, snow-free reflectance and transmittance properties of the phytoelements are calculated by weighting "live" and "dead" phytoelement optical property values, held in the time-invariant vegetation properties table for each species, by N and $(1 - N)$, respectively. These values, ρ_Λ and δ_Λ, are then adjusted for the effects of intercepted snow using (39) and (40), and the soil reflectance is similarly altered using (41). The radiative transfer submodel is then used to calculate the total amount of radiation absorbed by the canopy Rn_c and soil Rn_g.

(iii) The canopy and ground wetness fractions (i.e., the proportions of the canopy and ground that are covered in water or snow) and the soil surface resistance and humidity of the upper soil layer are calculated from (33) through (35). Canopy and ground thermal properties are calculated from equations in appendix E.

(iv) The aerodynamic resistances for the beginning of the time step are calculated. The adjusted values of z_0, d, C_1, and C_2 from (i) are used in (14), (15), and (16) to calculate r_b, r_d, and r_a.

(v) The canopy photosynthesis–conductance model is run in either its full-solution mode (off line) or in its time-stepped mode (in the GCM) using (17) through (26) and (9).

The calculations in (v) go through six iterations to converge on a solution for c_i. This loop is nested within a nonneutral aerodynamic transfer iterative calculation (four passes), which is used to converge on the value of r_a in (iv).

(vi) All the component terms of (1) and (2) are inserted; for example, the E_c terms are replaced by the sum of the E_{ct} and E_{ci} terms from (27) and (33a), respectively. These complete forms of (1) and (2), which describe the time-variation of the "fast" prognostic SiB2 variables T_c and T_g, and similar equations for the planetary boundary-layer temperature T_m and water vapor concentration q_m, are linked by the fluxes of sensible and latent heat and the aerodynamic resistances r_a, r_b, and r_d. These four equations have been

SUBROUTINE column (top, rotated): RBRD VNTLAT/RASITE*, PHOSIB, BEGTEM DELEF, DELHF, SIBSLV, ENDTEM, UPDAT2, RUN2, INTER2, ADDINC

EQUATION references (top): 14, 15, 16; Appendix C, 9, 17-26; 27, 33a, 34, 33b, Randall et al. (1996); 4-6, 7; 36-38; Appendix D; 1-9

Boxes (top row, right-hand section):

(iv) Aerodynamic resistances
r_b, r_d, r_a = f($\bar{C}_1$, $\bar{C}_2$, z_o, d, T_c, T_g, T_m)
(4 iterations)

(v) Calculate A_c, g_c
• Photosynthesis conductance model
(6 iterations)
• $r_c = 1/g_c$

(vi) Solution of 'fast' prognostic equations
• Expand (1) and (2)
$E_c = E_{ct} + E_{ci}$
$E_g = E_{gs} + E_{gi}$
• Differentiate (1), (2) and prognostic equations for T_m, q_m with respect to T_g, T_c, T_m, q_m
• Solve equation set for increments
ΔT_g, ΔT_c, ΔT_m, Δq_m

(vii) Calculation of provisional fluxes
• Use ΔT terms to increment fluxes
• Test to see if λE_c, λE_g change sign during ΔT; if so, λE_c or $\lambda E_g = 0$ and H_c or H_g is augmented
• Check for phase changes

(viii) Evapotranspiration extraction from stores
• Interception losses, soil evaporation
• Transpiration

(ix) Soil moisture interlayer exchanges, baseflow

(x) Interception of precipitation
Overland flow
Phase changes due to precipitation interception

(xi) Update prognostic variables, return final fluxes to atmosphere
$t = t + \Delta t$; Return to (i)

SUBROUTINE column (center): AERSET, MAPPER, SRFCHR/VEGINC*, SNOW1, RADAB, BEGTEM

EQUATION column (lower): Table 2, Sellers et al. (1995); Sellers et al. (1995); Appendix B; Sellers et al. (1995); Table 1c; Tables 1b, d; 42; 39, 40, 41; Appendix A; Appendix A; 33, 35; Appendix E

CALCULATION/PROCEDURE

OFFLINE

Read in SVI data, vegetation map
Use satellite data to generate monthly FPAR,
L_T, N, $\bar{k}$ for each grid square = f(SVI, Veg type)

Calculate aerodynamic properties
C_1, C_2, z_o, d = f(L_T, Veg type)
Generate table AEROSIB

Generate monthly tables of time-varying properties.
FPAR, L_T, N, $\bar{k}$
C_1, C_2, z_o, d

ONLINE

Read in boundary conditions: Time-varying properties
Read in time-invariant properties, etc.
Read in initial conditions

$t = t_0$

(i) Adjust aerodynamic properties
z_o, d, C_1, C_2 for snow accumulation

(ii) Radiative transfer calculations
• Calculate ρ, δ = f($ρ_{live,dead}$, $δ_{live,dead}$, N)
• Adjust ρ, δ, $ρ_{soil}$ for snow cover
• Calculate $\downarrow L$, $\downarrow T$ for F_{Λ}, μ
• Calculate Rn_c, Rn_g

(iii) Wetness fractions; specific heats
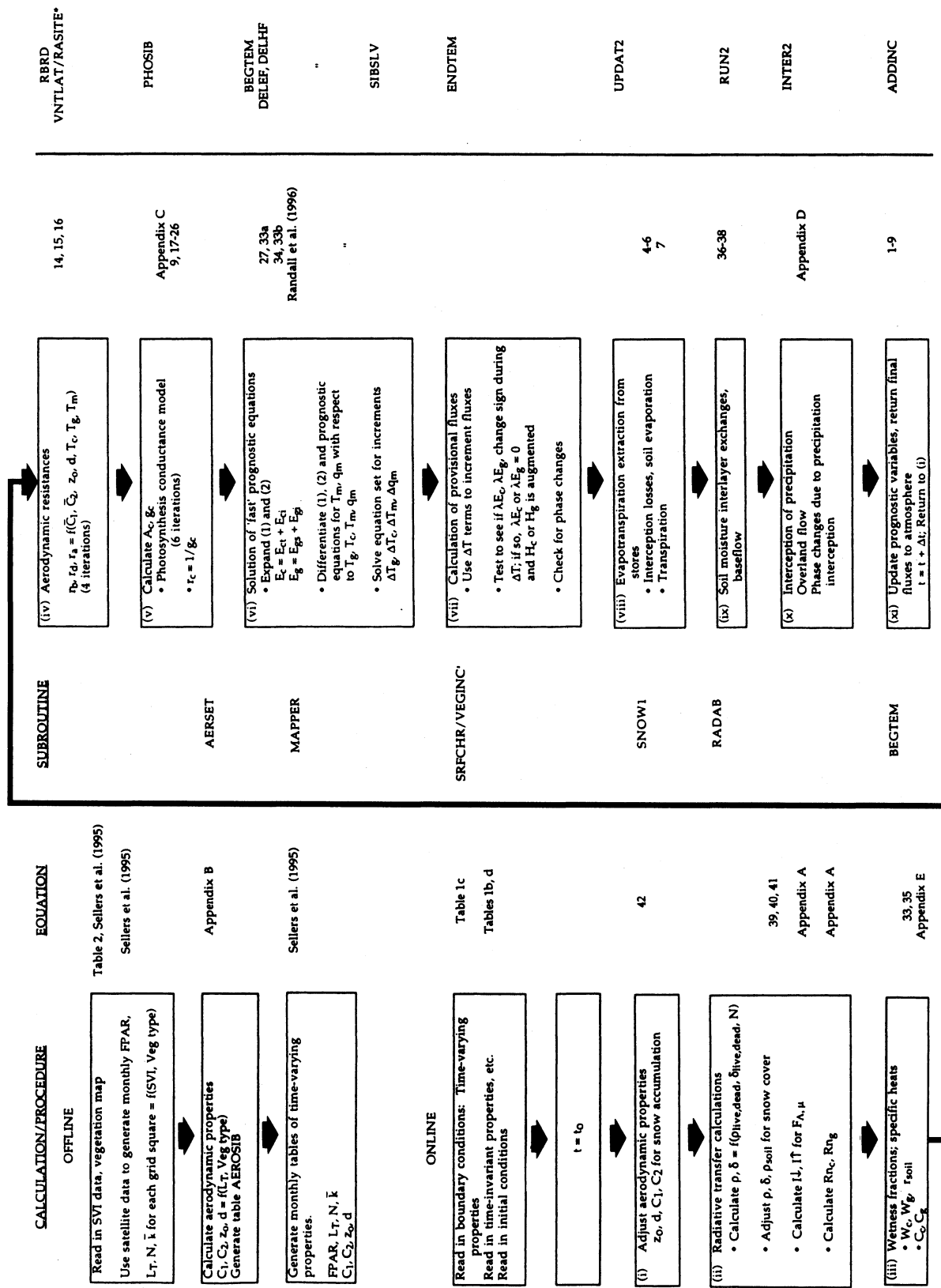• W_c, W_g, f_{soil}
• C_c, C_g

FIG. 7. Sequence of calculations used to advance the prognostic variables of SiB2 by one time step. Numbers in parenthesis refer to equations in text. Asterisk denotes subroutine used in off-line mode.

differentiated to provide partial derivatives of the flux terms; H_c, H_g, λE_c, λE_g, and the four prognostic variables (T_c, T_g, T_m, q_m) with respect to the four prognostic variables. The equations are then solved to yield the increments: ΔT_c, ΔT_g, ΔT_m, Δq_m.

(vii) The values of ΔT_c, ΔT_g, ΔT_m, and Δq_m are used to calculate provisional fluxes for the end of the time step. These are then used in a series of simple calculations to check for transitions from evaporation to condensation for the ground and canopy (in which case the latent heat flux for the relevant surface is set to zero and the excess energy dumped into sensible heat) and to account for the effects of phase changes. When this is done, the heat fluxes are finalized.

(viii) Evapotranspiration losses are extracted from the surface interception moisture stores (E_{ci} and E_{gi}), the soil surface (E_{gs}), or the root zone (E_{ct}) [see (4) through (7)].

(ix) Soil moisture fluxes between layers and baseflow runoff rates are calculated (see section 8). Soil moisture stores are updated.

(x) Precipitation is intercepted and apportioned to canopy and soil water surface runoff (see section 8).

(xi) The prognostic variables are updated, see (1) through (9), and the final values of fluxes are returned to the atmosphere. Diagnostic variables are calculated.

The fluxes returned to the atmosphere are described in appendices A and C but may be summarized as follows.

Reflected shortwave radiation:

$$F_{\Lambda,\mu(0)} - F_{\Lambda,\mu(c)} - F_{\Lambda,\mu(g)} \quad \text{for} \quad \Lambda = V, N; \mu = b, d$$

Emitted longwave radiation:

$$\sigma_s V \delta_T T_c^4 + \sigma_s(1 - V\delta_T T_g^4)$$

Latent heat fluxes:

$$\lambda E_c + \lambda E_g = \lambda E_{ct} + \lambda E_{ci} + \lambda E_{gs} + \lambda E_{gi}$$

Sensible heat fluxes:

$$H_c + H_g$$

CO_2 flux:

$$R_{\text{soil}} + R_D - A_c$$

Other net fluxes are described in appendices D and E but may be summarized as follows:

Runoff:

$$Ro_1 + Q_3$$

Canopy, soil heat fluxes:

$$C_c(\partial T_c/\partial t); \ C_g(\partial T_g/\partial t) + (2\pi C_d/\tau_d)(T_g - T_d)$$

Phase change energies:

$$\xi_c, \xi_{gs}$$

Details on the initialization of the prognostic variables in SiB2, in particular the soil moisture stores W_1, W_2, and W_3, may be found in Randall et al. (1996).

11. Summary and discussion

SiB2 incorporates a number of significant changes over the original version of SiB1 of Sellers et al. (1986). These include the incorporation of a more realistic canopy physiology model; specification of surface boundary conditions from satellite data; description of nonuniform snow cover; an improved hydrological formulation and reduction of the two-story vegetation in SiB1 to a single layer in SiB2.

The photosynthesis–conductance model used in SiB2 is a considerable improvement over the empirical stomatal model used in SiB1. Besides being more realistic, it requires the specification of a much smaller set of parameters (see Sellers et al. 1995). Additionally, the most important parameter in the new model, FPAR, can be specified relatively easily from satellite data.

The use of satellite data to describe vegetation phenology gives us much more confidence in the global parameter fields associated with SiB2 compared to SiB1. For example, this procedure immediately improved the calculation of surface albedo (see Sellers et al. 1996; Randall et al. 1996). The reduction of the two-story vegetation of SiB1 to a single layer in SiB2 was necessary to accommodate the photosynthesis–conductance model and the use of satellite data to specify canopy-state parameters.

The "patchy" snow formulation has yielded two benefits; first, more realistic representation of land surface albedo over the Northern Hemisphere continents in winter; second, more realistic surface reflectance, energy balance, and temperature transitions over thawing grid areas.

The improved hydrological formulation in SiB2 appears to have solved some persistent numerical problems associated with soil interlayer exchanges in SiB1. The revised base flow of Liston (1992, personal communication) should help to generate more developed and realistic seasonal cycles of soil moisture content.

The reduction in the number of parameters that need to be specified in SiB2 as compared with SiB1 is considerable. First, each vegetation type in SiB2 has much less than one-half the number of parameters, and second, many of these are shared with other vegetation types (see Sellers et al. 1996).

The main motivation for this work was to improve the realism of the model. In addition, the ability to calculate coupled energy, water, and carbon fluxes over the continents using plausible physiological models with boundary conditions specified from satellite observations, all within the context of an atmospheric GCM, holds promise for tackling some important earth science problems.

APPENDIX A

Two-Stream Approximation Radiative Transfer Model Used in SiB2

The original equations as specified by Dickinson (1983) are as follows:

$$-\bar{\mu}\frac{dI\uparrow}{dL} + [1 - (1 - \beta)\omega]I\uparrow$$
$$- \omega\beta I\downarrow = \omega\bar{\mu}K\beta_0 e^{-KL}, \quad (A1)$$

$$\bar{\mu}\frac{dI\downarrow}{dL} + [1 - (1 - \beta)\omega]I\downarrow - \omega\beta I\uparrow$$
$$= \omega\bar{\mu}K(1 - \beta_0)e^{-KL}, \quad (A2)$$

where

$I\uparrow, I\downarrow$ = upward and downward diffuse radiative fluxes, respectively, normalized by the incident flux;
μ = cosine of the zenith angle of the incident beam;
K = optical depth of the direct beam per unit leaf area,
$= G(\mu)/\mu$;
$G(\mu)$ = projected area of phytoelements in direction μ;
$\bar{\mu}$ = average inverse diffuse optical depth per unit leaf area;
β, β_0 = upscatter parameters for the diffuse and direct beams;
ω = scattering coefficient of phytoelements
$= \alpha + \delta$;
α = phytoelement reflectance coefficient;
δ = phytoelement transmission coefficient; and
L = cumulative leaf area index, m^2 m^{-2}.

The values of the parameters K, $G(\mu)$, $\bar{\mu}$ are functions of canopy geometry, specifically the leaf angle distribution function, and of μ, in the case of K and $G(\mu)$. The values of the upscatter parameters β and β_0 are functions of canopy geometric properties as well as phytoelement optical properties (see Dickinson 1983; Sellers 1985).

Determination of these parameters requires specification of the leaf angle distribution. In SiB1 and SiB2

this is done by means of the χ_L function of Ross (1975), whereby the departure of leaf angles from a spherical or random distribution is characterized by a simple expression:

$$\chi_L = \pm \int_0^{\pi/2} |1 - O(\theta)| \sin\theta d\theta, \quad (A3)$$

where

θ = the leaf inclination angle relative to a horizontal plane, and
$O(\theta)$ = leaf-angle distribution function.

Here $\chi_L = 0$ for spherically distributed leaves, $+1$ for horizontal leaves, and -1 for vertical leaves. Goudriaan (1977) fitted a curve to datasets generated from (A3), which provides reasonable estimates of the average leaf projection in any direction, given the value of χ_L:

$$G(\mu) = \phi_1 + \phi_2\mu; \quad (A4)$$
$$\phi_1 = 0.5 - 0.633\chi_L - 0.33\chi_L^2;$$
$$\phi_2 = 0.877(1 - 2\phi_1).$$

Equation (A4) may be used over the range $-0.4 < \chi_L < 0.6$. Field data have been analyzed to specify χ_L for different biomes; in the absence of other information $\chi_L = 0$ is assumed, and (A4) is then used in the calculation of $G(\mu)$, K, μ, β, and β_0. Term χ_L is also used to describe the aerodynamic properties of phytoelements (see appendix B).

The two equations (A1) and (A2) are solved using the incident (above canopy) radiation flux and the upwelling diffuse flux reflected by the soil as upper and lower boundary conditions, respectively. The calculation is performed for each of the four solar radiation components with a different simplified calculation for the exchanges of thermal infrared radiation. For the case of direct-beam visible or near-infrared solar radiation, the solutions to (A1) and (A2) are

$$I\downarrow = \alpha_1 e^{-KL} + \alpha_2 e^{-\alpha_3 L} + \alpha_4 e^{\alpha_3 L}, \quad (A5)$$
$$I\uparrow = \alpha_5 e^{-KL} + \alpha_6 e^{-\alpha_3 L} + \alpha_7 e^{\alpha_3 L}, \quad (A6)$$

where $\alpha_1, \alpha_2, \ldots \alpha_7$ are algebraic combinations of the coefficients in (A1) and (A2) (see the appendix of Sellers 1985). [Note: there is an error in the expression for α_5 in the appendix of Sellers et al. (1985), where α_5 is called h_4. The correct version is $h_4 = -f_{p3} - cd$.] The downward flux of diffuse radiation in the canopy $I\downarrow$, as described by (A5) has a component resulting from interception and rescattering of the direct beam radiation (first term), an exponentially extinguished downward flux resulting from downward scattering in the canopy (second term) and an exponentially attenuated upwards flux resulting from upward scattering of radiation by phytoelements and soil (third term). The terms in (A6) describe similar processes. From (A5) and (A6), $I\uparrow(0)$ can be calculated and subsequently

used as the canopy-soil system hemispherical reflectance, while $I\downarrow (L_T) + e^{-KL_T}$ defines the spectral transmittance of the vegetation. Similar equations can be defined to calculate the fate of incident diffuse fluxes (see the appendix of Sellers 1985).

The solar radiation absorbed by the canopy and ground is given by

$$F_{\Lambda,\mu(c)} = V[1 - I\uparrow_c - I\downarrow_g(1 - a_{s_{\Lambda,d}})$$
$$- e^{-KL_T/V}(1 - a_{s_{\Lambda,b}})]F_{\Lambda,\mu(0)} \quad (A7)$$

and

$$F_{\Lambda,\mu(g)} = \{(1 - V)(1 - a_{s_{\Lambda,\mu}}) + V[I\downarrow_g(1 - a_{s_{\Lambda,d}})$$
$$+ e^{-KL_T/V}(1 - a_{s_{\Lambda,b}})]\}F_{\Lambda,\mu(0)}, \quad (A8)$$

where

V = Canopy cover fraction;
$F_{\Lambda,\mu(0)}$ = incident radiant solar energy of wavelength interval Λ (V = visible or N = near-infrared; divided at 0.7 μm) and direction μ (d = diffuse, b = beam) (W m^{-2});
$F_{\Lambda,\mu(c)}$ = amount of $F_{\Lambda,\mu(0)}$ absorbed by the canopy (W m^{-2});
$F_{\Lambda,\mu(g)}$ = amount of $F_{\Lambda,\mu(g)}$ absorbed by the ground (W m^{-2});
$I_c^\uparrow$ = diffuse flux leaving top of canopy, (W m^{-2});
$I_g^\downarrow$ = diffuse flux leaving base of canopy, (W m^{-2});
$e^{-KL_T/V}$ = direct beam flux penetrating canopy, (W m^{-2}), = 0, for diffuse flux calculation;
L_T = total (area-averaged) leaf area index;
$a_{s_{\Lambda,\mu}}$ = soil reflectance (function of wavelength and angle), in SiB2 $a_{s_{\Lambda,\mu}}$ is assumed invariant with μ.

The net absorbed thermal radiation fluxes are given by

$$F_{T,d}(c) = F_{T,d(0)}V\delta_T - 2\sigma_s T_c^4 V\delta_T + \sigma_s T_g^4 V\delta_T \quad (A9)$$

and

$$F_{T,d(g)} = F_{T,d(0)}(1 - V\delta_T)$$
$$+ \sigma_s T_c^4 V\delta_T - \sigma_s T_g^4, \quad (A10)$$

where

$F_{T,d(0)}$ = incident thermal infrared radiation (TIR) (assumed to be all diffuse), (W m^{-2});
$V\delta_T$ = fraction of incident TIR absorbed by canopy;
$\delta_T = 1 - e^{-L_T/V\bar{\mu}}$;
σ_s = Stefan–Boltzmann constant (W m^{-2} K^{-4}).

In (A9) and (A10), ground and canopy emissivities are assumed to approach unity. The net radiation fluxes for canopy and ground are then given by

$$Rn_c = \sum_{\substack{\Lambda=V,N,T \\ \mu=b,d}} F_{\Lambda,\mu(c)} \quad (A11)$$

and

$$Rn_g = \sum_{\substack{\Lambda=V,N,T \\ \mu=b,d}} F_{\Lambda,\mu(g)}, \quad (A12)$$

where

V, N, T = visible, near-infrared and thermal wavelength intervals.

Note that there are only five components to be summed on the right-hand sides of (A11) and (A12) as $F_{T,b(0)} = 0$.

APPENDIX B

Turbulent Transfer Submodel of SiB2

The turbulent transfer submodel of SiB2 is an amalgam of the methods described in Sellers et al. (1986, 1989). The full equation set is reproduced here for reference.

The equation set describing the turbulent transfer profile under neutral conditions reads as follows.

a. Above the transition layer: $z > z_t$

Here

$$\tau = \rho K_m \frac{\partial u}{\partial z}; \quad (B1)$$

$$K_m = K_m^* = k u_*(z - d); \quad (B2)$$

$$= \frac{k^2 u(z - d)}{\log\left(\dfrac{z - d}{z_0}\right)};$$

where

τ = shear stress (kg m^{-1} s^{-2});
ρ = air density (kg m^{-3});
K_m = momentum transfer coefficient (m^2 s^{-1});
K_m^* = log-linear profile value of K_m (m^2 s^{-1});
k = von Karman's constant = 0.41;
u_* = friction velocity (m s^{-1});
u = wind speed (m s^{-1});
z = height (m);
d = zero plane displacement height (m);
z_0 = roughness length (m).

b. Within the transition layer: $z_2 < z < z_t$

Here (B1) still holds but K_m is augmented by

$$K_m = K_m^* \left[1 + (G_1 - 1)\left(\frac{z_t - z}{z_t - z_2}\right)\right]. \quad (B3)$$

The transition height itself is assumed to be a linear function of z_0, so that

$$z_t = z_2 + G_4 z_0. \quad (B4)$$

Equation (B3) allows K_m to decrease linearly from the augmented value of $G_1K_m^*$ at $z = z_2$ to $K_m = K_m^*$ at $z = z_t$. To maintain constant shear stress throughout the same layer, the wind velocity gradient must shift away from the log-linear profile [see (B1)], which holds above, within, and below the canopy.

c. Within the canopy air space (CAS): $z_1 < z < z_2$

Leaf area density varies according to two linear functions:

$$L_d = a_1 + b_2z, \quad (z_1 < z < z_c) \qquad \text{(B5a)}$$

and

$$L_d = a_2 + b_2z, \quad (z_c < z < z_2). \qquad \text{(B5b)}$$

These functions yield the triangular profile of leaf area density shown in Fig. 3. Given an estimate of total leaf area index (L_T) from satellite data, the constants a_1, a_2, b_1, and b_2 can be obtained from the solution of

$$\int_{z_1}^{z_2} L_d dz = L_T. \qquad \text{(B5c)}$$

Shear is absorbed by drag force interactions with the canopy elements

$$\frac{\partial \tau}{\partial z} = \rho \frac{C_l L_d}{p_s} u^2, \qquad \text{(B6)}$$

where

C_l = leaf drag coefficient;
L_d = leaf area density $(m^2 \, m^{-3})$;
p_s = leaf shelter factor.

Monteith (1973) reproduces data that show the dependence of the leaf drag coefficient, C_l, of isolated leaves on leaf inclination and dimension. A simple formula was fitted to these data:

$$C_l = 1.328 \left[\frac{2}{\text{Re}^{1/2}} \right] + 0.45 \, \overline{\sin\theta}^{1.6}, \qquad \text{(B7)}$$

where

$\overline{\sin\theta}$ = mean leaf inclination;
$\quad = [\int_o^{\pi/2} \frac{1}{2}(1 - \chi_L) \cos\alpha \, d\alpha]/\int_o^{\pi/2} d\alpha$;
$\quad = (1/\pi)(1 - \chi_L)$;
χ_L = Ross-Goudriaan leaf angle distribution function;
α = leaf azimuth angle;
Re = Reynolds number;
$\quad = uD_l/v$;
u = typical local wind speed $\approx 1 \, \text{m s}^{-1}$;
D_l = leaf dimension;
$\quad = (l_w + l_L)/2$;
l_w, l_L = leaf width, leaf length (m);
v = kinematic viscosity of air,
$\quad \approx 0.15 \times 10^{-4} \, \text{m}^2 \, \text{s}^{-1}$ @ 15°C.

The shelter factor p_s was first introduced by Thom (1972) and is still not well understood. It accounts for the observation that the drag coefficient of an ensemble of densely clustered phytoelements is less than the sum of their individual drag coefficients, presumably due to mutual sheltering effects. We have assumed that $p_s = 1$ when the leaf area density L_d is zero, that is, no shelter effect, and that $p_s = 4$ when $L_d = 6$, following the observations of Thom (1972). From these two data points and assuming that p_s must be a power relation, we use a mean value of p_s for the entire canopy given by

$$p_s = 1 + L_d^{0.6}. \qquad \text{(B8)}$$

Within the canopy K_m is assumed to be a product of local wind speed and a mixing length, l_m, which must be solved for

$$K_m = l_m u, \qquad \text{(B9)}$$

where

l_m = mixing length (m).

d. Below the canopy: $z < z_1$

A log-linear wind profile holds from z_1 to the soil surface:

$$\tau_1 = \rho \left[\frac{ku_1}{\log(z_1/z_s)} \right]^2, \qquad \text{(B10)}$$

where

τ_1 = shear stress at z_1 (and z_s) $(\text{kg m}^{-2} \, \text{s}^{-1})$;
u_1 = wind speed at z_1 (m s^{-1});
z_s = roughness length of soil/litter surface (m)
$\quad = 0.05$ m.

One last equation describes the zero-plane displacement height d as the moment height for momentum absorption, following Thom (1971):

$$d = \frac{\int_{z_1}^{z_2} C_B u^2 z dz}{\int_{z_1}^{z_2} C_B u^2 dz + \dfrac{\tau_1}{\rho}}, \qquad \text{(B11)}$$

where

$$C_B = L_d C_l / p_s.$$

The equation set is solved by matching boundary conditions at z_t, z_2, z_c, and z_1.

First, (B5) and (B7) are inserted into (B6), which is combined with (B1) and (B9) to yield an expression for the wind profile within the canopy $(z_1 < z < z_2)$:

$$\frac{d^2}{dz^2} (u^2) = (A_i + B_i z)u^2, \qquad \text{(B12)}$$

where

$$A_i = \frac{2a_i C_l}{p_s l_m};$$

$$B_i = \frac{2b_i C_l}{p_s l_m};$$

$i = 1$ or 2, depending on whether $z \lessgtr z_c$.

Equation (B12) may be solved to give an expression for the wind profile within the canopy air space (CAS) that incorporates the modified Bessel function, $I_{1/3}$, and the modified Bessel function of the second kind (the MacDonald function), $K_{1/3}$:

$$u^2 = Y_\alpha \alpha_i + Y_\beta \beta_i, \qquad (B13)$$

where

$$Y_\alpha = \sqrt{\eta} I_{1/3}(\xi);$$
$$Y_\beta = \sqrt{\eta} K_{1/3}(\xi);$$
$$\eta = B_i^{-2/3}(A_i + B_i z);$$
$$\xi = \frac{2}{3}\eta 3/2.$$

Here α_i, β_i are constants determined from the solution of (B13) with the boundary conditions. Equation (B13) may be manipulated further to yield expressions for the gradient of wind speed within the canopy air space (CAS) in terms of positive indexes as required by IMSL (1984) subroutines that are used to solve the equation set [see the appendix of Sellers et al. (1989) for further details].

The equation set is combined and solved to yield the bulk aerodynamic characteristics of the vegetated surface in the offline MOMOPT program. Manipulation of (B1), (B2), (B3), (B10), and (B13) and matching their boundary conditions at z_t, z_2, z_c, and z_1 yields solutions for z_o, d, and profiles of u and K_m, given input values of G_1, G_4, z_2, z_c, z_1, L_T, C_l, and z_s. The values of $G_1 = 1.449$ and $G_4 = 11.785$ were determined for SiB1 by optimizing the calculated values of z_o and d derived by this model against values of z_o and d calculated by the second-order closure model of Shaw and Pereira (1982) (see Sellers et al. 1989). These values have been retained for SiB2.

APPENDIX C

Photosynthesis-Conductance Submodel of SiB2

a. Leaf-scale equation set and canopy integration technique

The Collatz et al. (1991) version of the model for C3 species describes the leaf assimilation (or gross photosynthetic) rate as the minimum of three limiting rates, w_c, w_e, w_s, which are functions that describe the assimilation rates as limited by the efficiency of the photosynthetic enzyme system (Rubisco-limited); the amount of PAR captured by the leaf chlorophyll, and the capacity of the leaf to export or utilize the products of photosynthesis, respectively.

For C4 species, the terms w_c and w_e still refer to Rubisco and light limitations, respectively, but w_s now refers to a PEP-Carboxylase limitation (see Collatz et al. 1992):

$$w_c = V_m \left[\frac{c_i - \Gamma^*}{c_i + K_c(1 + O_2/K_o)} \right], \quad \text{for C}_3, \quad (C1)$$

$$= V_m, \quad \text{for C}_4, \qquad (C2)$$

where

w_c = Rubisco-limited rate of assimilation (mol m^{-2} s^{-1});

V_m = maximum catalytic capacity of Rubisco (mol m^{-2} s^{-1});

c_i = partial pressure of CO_2 in leaf interior (Pa);

O_2 = partial pressure of O_2 in leaf interior (Pa);

Γ^* = CO_2 compensation point (Pa) = $0.5\, O_2/S$;

S = Rubisco specificity for CO_2 relative to O_2;

K_c = Michaelis-Menten constant for CO_2, (Pa);

K_o = inhibition constant for O_2, (Pa).

Here V_m is given by the product of V_{max}, a temperature-dependent function and a soil moisture stress function [see (C17)]. Term V_{max} is a physiological property of the leaf (or chloroplast) and is proportional to the Rubisco reserves of the leaf (or chloroplast) and thus its nitrogen content. Terms S, K_c, and K_o are all functions of temperature [see the appendix of Collatz et al. (1991) and (C17)].

The light-limited rate of assimilation w_e is given by

$$w_e = (\mathbf{F}_\pi \cdot \mathbf{n})\epsilon_3(1 - \omega_\pi)\left[\frac{c_i - \Gamma^*}{c_i + 2\Gamma^*} \right], \quad \text{for C}_3, \quad (C3)$$

$$= (\mathbf{F}_\pi \cdot \mathbf{n})\epsilon_4(1 - \omega_\pi), \quad \text{for C}_4, \qquad (C4)$$

where

$\mathbf{F}_\pi$ = (vector) flux of PAR incident on the leaf (W m^{-2});

$\mathbf{n}$ = vector of leaf normal;

w_e = light-limited rate of assimilation (mol m^{-2} s^{-1});

$\epsilon_{3,4}$ = intrinsic quantum efficiency for CO_2 uptake (mol mol^{-1} or mol); J^{-1}; for C3, C4 photosynthesis, respectively;

ω_π = leaf-scattering coefficient for PAR ($\omega_\pi \approx \omega_v$).

A third limiting rate has been defined for C3 and C4 photosynthesis by Collatz et al. (1991, 1992), respectively: w_s is viewed as the capacity for the export or utilization of the products of photosynthesis in the case of C3 and as the CO_2-limited capacity for C4 photosynthesis.

Here

$$w_s = V_m/2, \quad \text{for C}_3, \qquad (C5a)$$

$$= 2 \times 10^4 V_m c_i / p, \quad \text{for C}_4, \qquad (C5b)$$

where

p = atmospheric pressure (Pa).

The simplest way to proceed is to assume that the assimilation rate is the minimum of w_c, w_e, and w_s (cf. Farquhar et al. 1980). However, observations indicate that the transition from one limiting rate to another is not abrupt and that coupling between the three processes leads to smooth curves rather than superpositioning of straight lines. Collatz et al. (1991) describe this effect by combining the rate terms into two quadratic equations, which are then solved for their smaller roots:

$$\beta_{ce} w_p^2 - w_p(w_c + w_e) + w_e w_c = 0, \quad \text{(C6a)}$$

$$\beta_{ps} A^2 - A(w_p + w_s) + w_p w_s = 0, \quad \text{(C6b)}$$

where

A = assimilation rate (mol m^{-2} s^{-1});
β_{ce}, β_{ps} = coupling coefficients;
w_p = "smoothed" minimum of w_c and w_e (mol m^{-2} s^{-1}).

The coefficients β_{ce} and β_{ps} can theoretically range from 1 (no coupling effects) to 0. In nature, these coefficients assume values on the order of 0.8 to 0.99 (see Collatz et al. 1990; Sellers et al. 1992a).
Net assimilation, A_n, is then given by

$$A_n = A - R_d, \quad \text{(C7)}$$

where

R_d = leaf respiration rate (mol m^{-2} s^{-1}).

Collatz et al. (1991, 1992) scaled R_d to the leaf carboxylase content by

$$R_d = f_d V_m, \quad \text{(C8)}$$

where

$f_d = 0.015$ for C$_3$,
　$= 0.025$ for C$_4$.

Collatz et al. (1991) went on to incorporate the above photosynthesis model with the Ball (1988) semi-empirical model for leaf stomatal conductance:

$$g_s = m \frac{A_n}{c_s} h_s p + b, \quad \text{(C9)}$$

where

g_s = stomatal conductance for water vapor (mol m^{-2} s^{-1} or m s^{-1});
m = coefficient from observations,
　≈ 9 for C$_3$ plants,
　≈ 4 for C$_4$ plants,
　≈ 6 for conifers;
b = coefficient from observations (mol m^{-2} s^{-1} or m s^{-1}),
　≈ 0.01 for C$_3$ plants,

　≈ 0.04 for C$_4$ plants;
h_s = relative humidity at leaf surface;
c_s = CO$_2$ partial pressure at leaf surface (Pa);
p = atmospheric pressure (Pa);
g_s (m s^{-1}) = 0.0224 $(T/T_f)(p_o/p)g_s$ (mol m^{-2} s^{-1});
p_o = standard atmospheric pressure (Pa);
　$= 1.013 \times 10^5$;
T_f = freezing temperature = 273.16 K.

The leaf surface environment variables h_s and c_s are given by (see Fig. 4)

$$E_{lt} = g_l(e_s - e_a)\frac{\rho c_p}{\lambda\gamma} = g_s(e_i - e_s)\frac{\rho c_p}{\lambda\gamma}. \quad \text{(C10a)}$$

We also see from Fig. 4 that

$$h_s = \left[\frac{e_s}{e_i}\right], \quad \text{(C10b)}$$

$$A_n = \frac{(c_a - c_s)}{p}\frac{g_l}{1.4} = \frac{(c_s - c_i)}{p}\frac{g_s}{1.6}, \quad \text{(C10c)}$$

where

e_a, e_s, e_i = water vapor partial pressure in the external air, at the leaf surface and inside the leaf (saturated), respectively (Pa);
$e_i = e^*(T_c)$ (Pa);
c_p = specific heat of air (J kg^{-1} K^{-1});
γ = Psychrometric constant (Pa K^{-1});
g_l = one sided leaf boundary layer conductance for water vapor (mol m^{-2} s^{-1} or m s^{-1}),
　$= 1/(2r_l)$, see Fig. 4;
E_{lt} = leaf transpiration rate (kg m^{-2} s^{-1});
c_a, c_s = carbon dioxide partial pressure in the external air and at the leaf surface, respectively (Pa);
1.4, 1.6 = factors to account for different diffusivities of H$_2$O and CO$_2$ in the leaf boundary layer and stomatal pores, respectively.

The system is then closed by calculating the CO$_2$ partial pressure of the leaf interior:

$$c_i = c_s - \frac{1.6 A_n}{g_s}p. \quad \text{(C11)}$$

Sellers et al. (1992a) describe how the system of equations (C1) through (C11) can be solved for steady-state conditions, that is, assuming no biochemical or mechanical lags in stomatal function. The procedure requires up to five iterations through the equation set (see Fig. 4 of Sellers et al. 1992a) and is suitable for all off-line applications, especially when the timestep is longer than a few minutes. This method was incorporated in the off-line version of SiB2 distributed in late 1993. A more efficient solution method was developed for use within the GCM of Randall et al. (1996), which is based on a prognostic equation for leaf–canopy conductance, summarized in (9) and at the end of this appendix.

The equation set reviewed above is relevant to a single leaf with known physiology (V_{max}, ϵ, m), physical properties (ω_v, C_s, χ_L), and forcing conditions (T_c, PAR, e_a, u). The next step is to integrate the equation set to describe canopy photosynthesis A_c and conductance g_c.

The analysis and observations discussed earlier in this paper and in more detail in Sellers et al. (1992a) support the hypothesis that the depth-profile of leaf nitrogen V_{max}, and hence V_m, within the canopy are distributed according to the radiation-weighted, time-mean profile of PAR. For the PAR wavelength interval, a simple exponential description of radiation attenuation can be used to describe the profile of PAR and, in averaged form, the profile of V_{max} (see Sellers 1985, 1987). Thus,

$$V_{max_L} = V_{max_0} e^{-\bar{k}L}, \qquad (C12)$$

$$\mathbf{F}_\pi \cdot \mathbf{n} \approx F_{\pi_0}\left[\frac{\overline{G(\mu)}}{\mu}\right] e^{-\bar{k}L}, \qquad (C13)$$

$$\bar{k} = \left[\frac{\overline{G(\mu)}}{\mu}\right][1 - \omega_\pi]^{1/2}, \qquad (C14)$$

where

V_{max_L}, V_{max_0} = value of V_{max} at leaf area index (LAI) of L and at the top of the canopy (LAI = 0), respectively (mol m^{-2} s^{-1});

F_{π_L}, F_{π_0} = value of PAR flux at LAI = L and top of the canopy, respectively (W m^{-2});

F_{π_0} = $F_{v,d_0} + F_{v,b_0}$ (W m^{-2});

$\bar{k}$ = time–mean radiation-weighted value of the PAR extinction coefficient.

Equation (C12) describes a time-mean profile of V_{max}, which can be assumed to be invariant over periods of a few days or weeks. The same time–mean profile is assumed for the instantaneous extinction of PAR in (C13), whereas in reality, this profile could change considerably over the course of a day. However, numerical experiments in Sellers et al. (1992a) showed that the simplifications inherent in (C13), that is, $F_{\pi_0} = F_{v,d_0} + F_{v,b_0}$ and $k \approx \bar{k}$, do not generate large errors.

The equations for leaf-level photosynthesis and conductance can now be integrated over the depth of the canopy to yield bulk canopy values of A_c, g_c, c_i, and h_s. This is done by

(i) inserting (C12) into (C1), (C2), and (C5) via the $V_m = f(V_{max})$ relationship of (C17);

(ii) inserting (C13) into (C3) and (C4);

(iii) providing canopy-integrated values of R_d (by integrating V_m over the canopy depth) in (C8) and g_l, [by using $1/r_b$, see (10), (15)]; and

(iv) assuming common or bulk values of c_i, c_s, and h_s.

Essentially, these substitutions relate the activity of all leaf layers in the canopy to the performance of the top leaves through the $e^{-\bar{k}L}$ terms. When this

is done and the resulting expressions are fed into (C6), all the terms are found to be the product of "top" leaf properties and PAR fluxes (V_{max_0}, F_{π_0}), bulk canopy terms (c_I, c_S, h_S), and an $e^{-\bar{k}L}$ term. To obtain estimates of A_c and g_c, the $e^{-\bar{k}L}$ term is removed and integrated separately over the depth of the canopy. If we now include the effects of vegetation clumping ($V < 1$) and the inclusion of nongreen material ($N < 1$), this gives

$$A_c = A_{n_0}\int_0^{L_T/V} VN e^{-\bar{k}L}dL = A_{n_0}\Pi \qquad (C15)$$

$$\Pi = \frac{VN(1 - e^{-\bar{k}L_T/V})}{\bar{k}}$$

$$\Pi \approx FPAR/\bar{k}$$

$$A_{n_0} = A_n \text{ for top green leaves}$$

$$g_c = m\frac{A_c}{c_S}h_S p + bL_T. \qquad (C16)$$

These expressions for A_c and g_c roughly correspond to their leaf-level analogs for the top leaves in the canopy multiplied by the canopy PAR use term, Π, which is taken as equal to FPAR/$\bar{k}$.

The replacement of individual leaf-level terms by bulk canopy terms or terms relating leaf performance to conditions at the top of the canopy can be done quite simply for (C1) through (C11), which are then solved to calculate A_c and g_c in the same way as was done for A and g_s. The canopy transpiration rate E_{ct} is obtained by modifying (C10a): replacement of g_l by $1/(2r_b)$ and g_s by g_c converts E_{lt} to E_{ct}. Sellers et al. (1992a) compared results from this greatly simplified bulk canopy approach, with results obtained from an equivalent multilayer numerical model capable of reproducing highly developed and variable profiles of PAR, c_i, c_s, and h_s. The values of A_c, g_c, and the bulk terms for c_i, c_s, R_d, and h_s calculated by the two schemes were found to match closely under all but the most extreme and unrealistic conditions.

Equations (C1) through (C16) describe the transfers of CO_2 between the canopy interior CO_2 sink c_I and the canopy air-space source c_a. When SiB2 is coupled with a GCM, c_a is defined as a function of the CO_2 concentration at the reference height, c_m, the flux from the canopy, $A_c - R_D$, a respiration flux from the soil, R_{soil}, and the connecting resistances r_c, r_a, r_b, and r_d; see Fig. 2 and Table 4. In the absence of a soil-respiration formulation, R_{soil} was set to zero in the Randall et al. (1996) GCM study.

Equations (C1) through (C11) include functions that describe the effects of temperature (through the expressions for V_m, K_c, K_o, S) and the stomatal closure response when exposed to dryer air through the h_s term in (C9). Soil moisture stress is applied to the calculation of V_m and hence R_d, w_c, and w_s in (C6) and (C8) in a simple empirical way:

$$V_m = V_{max}f_T(T_c)f_w(W_2), \qquad (C17)$$

$$K_c = 30 f_T(T_c),$$

$$K_0 = 30\,000 f_T(T_c),$$

$$S = 2600 f_T(T_c),$$

$$f_T(T_c) = 2Q_t/\{1 + \exp[s_1(T_c - s_2)]\}, \quad \text{for } C_3 V_m,$$

$$= 2Q_t/\{1 + \exp[s_1(T_c - s_2)]\}$$

$$\times \{1 + \exp[s_3(s_4 - T_c)]\}, \quad \text{for } C_4 V_m,$$

$$= 2Q_t/\{1 + \exp[s_5(T_c - s_6)]\}, \quad \text{for } R_d V_m,$$

$$= 2.1Q_t, \quad \text{for } K_c,$$

$$= 1.2Q_t, \quad \text{for } K_0,$$

$$= 0.57Q_t, \quad \text{for } S,$$

$$Q_t = Q_{10} \text{ coefficient},$$

$$= (T_c - 298)/10,$$

$$f_W(W_2) = 1/\{1 + \exp[0.02(\psi_c - \psi_r)]\},$$

ψ_c = critical water potential (m),
ψ_r = root zone soil moisture potential (m),
$\quad = \psi_s W_2^{-B}$,
ψ_s = value of soil moisture potential at saturation (m),
B = empirical parameter,
s_i = high and low temperature inhibition parameters.

The soil moisture stress factor is also used to scale b in (C16).

In the C_3 model, a cold temperature inhibition term is applied to w_s in (C5). In the C_4 model, it is applied directly to V_{max} in (C17). Some of the temperature inhibition parameters depend on vegetation type (see Sellers et al. 1996). The parameters ψ_s and B are dependent on soil type and are discussed in more detail in section 8 and in Sellers et al. (1996).

b. Canopy-integrated photosynthesis-conductance equations

The components of the canopy-scale photosynthesis–conductance equations are defined as follows in SiB2:

canopy biophysical rate variable

= | leaf physiology or radiation rate limit (top leaves) |

$\times$ | environmental forcing or feedback terms |

$\times$ | canopy PAR use parameter |

$$A_c, f g_c = |V_{max_0}, F_0| |B_1 \cdots B_6| |\Pi| \quad \text{(C18)}$$

$$w_C = V_{m_0} \Pi B_1, \quad \text{(C19)}$$

$$w_E = F_{\pi_0} \Pi B_2, \quad \text{(C20)}$$

$$w_S = V_{m_0} \Pi B_3, \quad \text{(C21)}$$

$$R_D = V_{m_0} \Pi B_4, \quad \text{(C22)}$$

$$A_c = A_{n_0} \Pi B_5 = f(w_C, w_E, w_S) - R_D, \quad \text{(C23)}$$

$$g_c \approx A_{n_0} \Pi B_6, \quad \text{(C24)}$$

$$\Pi = \text{FPAR}/\bar{k} \approx VN[1 - \exp(-\bar{k}L_T/V)]/\bar{k}, \quad \text{(C25)}$$

where

$$B_1 = \left[\frac{c_I - \Gamma^*}{c_I + K_c[1 + O_2/K_o]}\right], \quad \text{for } C_3,$$

$$= 1, \quad \text{for } C_4,$$

$$B_2 = \overline{\left[\frac{G\mu}{\mu}\right]}(1 - \omega_\pi)\epsilon_3, \left[\frac{c_I - \Gamma^*}{c_I + 2\Gamma^*}\right], \quad \text{for } C_3,$$

$$= \overline{\left[\frac{G\mu}{\mu}\right]}(1 - \omega_\pi)\epsilon_4, \quad \text{for } C_4,$$

$$B_3 = 0.5, \quad \text{for } C_3,$$

$$= 2 \times 10^4 c_I/p, \quad \text{for } C_4,$$

$$B_4 = f_d,$$

$$B_5 = 1.0,$$

$$B_6 = \frac{m h_s p}{c_S}.$$

The leaf-scale variables in section 7 and in (C1) through (C11) have been replaced by canopy-scale variables, denoted by capital subscripts, in the equation set above (see Sellers et al. 1992a).

c. Time-stepping scheme for canopy conductance, g_c

The physiological processes that determine A_c and g_c do not respond instantaneously to perturbations in the driving variables. Photosynthesis usually approaches steady state within a minute for a step change in conditions, while stomatal conductances take several minutes to reach steady state. The current CSU GCM implementation of SiB2 operates at a time step on the order of minutes, which means that A_c requires a numerical solution for steady state (see section 7a), while g_c is more realistically modeled as lagging behind the steady state for a time step. The lag in stomatal response is modeled as a simple restricted growth process:

$$\frac{\partial g_c}{\partial t} = -k_g(g_c - g_{c_{inf}}), \quad \text{(C26)}$$

k_g = time constant for stomatal response,
$\quad = 0.00113 \text{ s}^{-1}$,
$g_{c_{inf}} = g_c \quad \text{as} \quad t \to \infty$,
$\quad = m \dfrac{A_c}{c_S} h_s p + b.$

The solution to this equation is

$$g_c = e^{-k_g t} g_{c_0} + (1 - e^{-k_g t}) g_{c_{inf}}$$

$$g_{c_0} = g_c \quad \text{at} \quad t = 0. \quad \text{(C27)}$$

The change in g_c over the time step Δt is then defined as

$$\Delta g_c = g_c - g_{c_0} = (1 - e^{-k_g \Delta t})(g_{c_{\inf}} - g_{c_0}). \quad \text{(C28)}$$

APPENDIX D

Precipitation and Interception Loss

In SiB2, we assume that the convective rainfall amount is spatially distributed, as shown in Fig. 5 and as given by

$$I_c(x) = a_c e^{-b_c x} + c_c, \quad \text{(D1)}$$

where

$I_c(x)$ = relative amount of convective precipitation as a function of fractional area of grid area x, $(0 < x < 1)$, falling within the time step;

a_c, b_c, c_c = constants (see Fig. 5),
= 20, 20, 0.206 $\times$ 10^{-8}, respectively.

The constants a_c, b_c, c_c were obtained by comparison with the data of Ruprecht and Gray (1976) and are normalized so that

$$\int_0^1 I_c(x)dx = 1. \quad \text{(D2)}$$

Equation (D1) can be rewritten (with subscript "l") to represent large-scale spatially uniform precipitation by use of the coefficients $a_l = 0.0001$, $b_l = 20$, and $c_l = 0.9999$, which means that in the interval $0 < x < 1$, $I_l(x) \approx 1$. Both types of precipitation (most models can produce both types simultaneously) can then be combined to give a single area–amount function by

$$PI_{(x)} = (P_c a_c + P_l a_l)e^{-bx} + (P_c c_c + P_l c_l), \quad \text{(D3)}$$

where

P = total precipitation during a time step (m),
= $P_c + P_l$,
P_c, P_l = convective, large-scale rainfall during a time-step, respectively (m).

Term $PI_{(x)}$ is a total amount distribution which can be used to calculate throughfall rates and infiltration excess.

The direct throughfall component, the rainfall that falls through the gaps in the canopy, is calculated by a modification of the radiation formulation:

$$D_d = \delta_p P, \quad \text{(D4)}$$

where

D_d = direct throughfall (m);
δ_p = canopy throughfall coefficient,
= $1 - V + Ve^{-K_p L_T / V}$;
K_p = extinction coefficient for rainfall, same as for a vertical beam of radiation;
= $G(\mu)/\mu$, $\mu = 1$.

The rainfall intercepted, but not necessarily retained, by the canopy is then given by $P - D_d$. The proportion of the grid area for which the canopy has intercepted enough rainfall to equal or exceed its saturation limit x_s is given by the solution to

$$PI_{(x_s)} = S_c - M_{cs} - M_{cw}, \quad \text{(D5)}$$

where

S_c = canopy storage limit (m),
= $0.0001 L_T$.

Figure 5b shows how the precipitation area-amount function is added to the water or snow already stored on the canopy (which is assumed to be uniformly distributed at the beginning of the time step) and shows how x_s relates to S_c. Combining (D5) with (D3), we have

$$x_s = \frac{-1}{b} \log\left[\frac{S_c - M_{cs} - M_{cw}}{a_p(1 - \delta_p)P} - \frac{c_p}{a_p} \right], \quad \text{(D6)}$$

where $a_p = (P_c a_c + P_l a_l)/P$ and so forth for c_p. Reference to Fig. 5b shows the physical significance of x_s and how it is used to calculate the canopy drainage term D_c,

$$D_c = \int_0^{x_s} PI(x)dx - (S_c - M_{cs} - M_{cw})x_s$$

$$= P(1 - \delta_p)\frac{a_p}{b}(1 - e^{-bx_s})) + c_p x_s$$

$$- (S_c - M_{cs} - M_{cw})x_s. \quad \text{(D7)}$$

The additional amount of water remaining on the canopy, that is, available for direct evaporation (interception loss) is given by

$$\Delta M_{cs,w} = P - D_c - D_d, \quad \text{(D8)}$$

$\Delta M_{cs,w}$ = change in canopy water storage amount (m).

From then on, the intercepted water is assumed to be uniformly spread over the vegetation canopy, which is clearly inconsistent with the representation shown in Fig. 5. However, we can assume that the resulting errors are small since the nonuniformity of intercepted precipitation will only determine the timing of evaporation loss unless convective storms are immensely concentrated in time and space.

The ground is assumed to have a surface "puddle" storage with a maximum liquid capacity S_g of 0.2 mm for M_{gw} and no upper limit for snow storage M_{gs}. A similar calculation to that shown in (D1) through (D8) is performed so that an effective precipitation rate reaches the soil surface (i.e., when S_g is exceeded by M_{gw}).

With very heavy rainfall, the local infiltration capacity of the soil can be "beaten" by the rainfall rate and (infiltration excess) overland flow can be generated.

For the sake of simplicity, we assume the same area–amount relationship for the rainfall (in fact, this would have been distorted by interception in the canopy, etc.). The soil hydraulic conductivity for the surface layer is used to calculate a water absorption rate for the top soil layer:

$$P_{W_1}(\text{max}) = K, \qquad (D9)$$

where

$P_{W_1}(\text{max})$ = input rate of liquid precipitation that soil can absorb during the time step (m s^{-1}),

K = soil hydraulic conductivity (m s^{-1}).

The fraction of the grid area giving rise to infiltration excess is then calculated by solving for $I(x_i)$ in

$$D_s I(x_i) = P_{W_1}(\text{max}), \qquad (D10)$$

where

D_s = amount of throughfall and vegetation drainage reaching the soil surface (m),

$\quad = D_c + D_d.$

The infiltration excess runoff rate, Ro_1, is then given by

$$\text{Ro}_1 = \int_0^{x_i} D_s I_{(x)} dx - K, \qquad (D11)$$

where the term inside the integral is similar to that in (D7).

When snow falls, equations (D2) through (D8) are used with the adjustment that all convective precipitation is added to and treated like large-scale rainfall in (D3). Equations (D9) through (D11) are not used; that is, the snow can build up and fall off the vegetation (when $M_{cs} > S_c$) but accumulates on (and does not run off until melted) the ground.

Once the precipitation has been intercepted by the canopy or ground, some calculations must be made to take account of possible phase changes. The canopy moisture stores M_{cw} or M_{cs} and the canopy itself are at a specified temperature T_c prior to the interception of precipitation at temperature T_m.

The equation used to calculate the change in canopy temperature due to interception ΔT_{ci} is given by

$$T_c C_{cm} + T_m \Delta C_{cm} = (T_c + \Delta T_{ci})$$
$$\times (C_{cm} + \Delta C_{cm}) + \epsilon_c / \rho_w, \qquad (D12)$$

where

C_{cm} = specific heat of canopy (leaves plus $M_{cw,s}$) prior to interception,

$\quad = (M_{cw} + M_{cs})C_w + L_T C_L;$

C_w = specific heat of water $(\text{J kg}^{-1} \text{K}^{-1})$;

C_L = specific heat of foliage $(\text{J kg}^{-1} \text{K}^{-1})$,

$\quad \approx 0.1 L_T C_W;$

ΔC_{cm} = change in canopy specific heat due to interception $(\text{J kg}^{-1} \text{K}^{-1})$;

$\quad = (P - D_c - D_d)C_w \, (\text{J kg}^{-1});$

ϵ_c = energy released or absorbed by phase changes (J m^{-2});

ρ_w = density of water (1000 kg m^{-3}).

In (D12) the "ϵ_c/ρ_w" term incorporates the units change from meters, used for precipitation interception, to kilograms, used for energy exchange calculations. If T_c and T_m are on either side of T_f (freezing temperature) at the beginning of the time step, some phase change is inevitable. Equation (D12) is used to determine the energy available for melting or freezing the canopy water–snow store or intercepted precipitation, along with the change in ΔT_{ci}.

The temperature and phase changes of the snow-covered ground are calculated by balancing the left-hand side (before interception) with the right-hand side (after interception) of (D13):

$$T_m(D_c + D_d)C_w + T_{\text{snow}}(\min(0.05, M_{gs})C_w + C_d A_s)$$
$$+ T_g C_d(1 - A_s) = (T_{\text{snow}} + \Delta T_{\text{snow}}) + (T_g + \Delta T_{gi})$$
$$\times (1 - A_s - \Delta A_s)C_d + \epsilon_g / \rho_w [\min(0.05, M_{gs})C_w$$
$$+ \Delta M_{gs} C_w + C_d(A_s + \Delta A_s)], \qquad (D13)$$

where

A_s = snow covered area;

a_s = 13.2 (m^{-1});

$\Delta A_s = a_s \Delta M_{gs}, \, 0 < A_s + \Delta A_s < 1;$

ϵ_g = energy due to phase changes $(\text{J kg}^{-1} \text{m}^{-1})$;

C_d = effective heat capacity of snow-free soil $(\text{J m}^{-1} \text{K}^{-1})$.

APPENDIX E

Soil Thermal Properties

Soil thermal properties are defined after Camillo and Schmugge (1981):

$$H_s = \left[\frac{1.5(1 - \theta_s) + 1.3\theta_s W_1}{0.75 + 0.65\theta_s - 0.4\theta_s W_1} \right] 0.4186, \qquad (E1)$$

$$C_{\text{soil}} = [0.5(1 - \theta_s) + \theta_s W_1]0.4186 * 10^7, \qquad (E2)$$

$$C_g = 0.5 \left(\frac{H_s C_{\text{soil}} \tau_d}{\pi} \right)^{1/2}$$
$$+ \min(0.05, (M_{gs} + M_{gw}))C_w, \qquad (E3)$$

where

W_1 = surface soil layer wetness;

θ_s = soil porosity;

H_s = soil thermal conductivity $(\text{W m}^{-1} \text{K}^{-1})$;

C_{soil} = soil specific heat $(\text{J m}^{-3} \text{K}^{-1})$;

C_g = effective heat capacity of surface (diurnally-responsive) soil layer and snow $(\text{J m}^{-2} \text{K}^{-1})$;

C_w = specific heat of water (J kg^{-1});

τ_d = daylength (s).

Here

$$C_d = 0.5\left(\frac{H_s C_{\text{soil}} T_d}{\pi}\right)^{1/2}, \qquad \text{(E4)}$$

where

C_d = effective heat capacity of snow-free soil, ($\text{J m}^{-2}\text{ K}^{-1}$).

Note that the effective soil heat capacity for the upper (diurnally responsive) soil layer takes some account of snow accumulation [see (E3)]. Conduction of heat from the upper layer to the deeper (seasonally responsive) soil layer is a function of soil properties only [see (E4) and (2) and (3) in Table 3]. This modification of the Deardorff (1977) force-restore formulation is very crude and does not realistically describe the insulating effects of snow. We intend to replace this part of the model with a multilayer soil heat and moisture flux model, with a separate layer for snow, in the near future.

The canopy specific heat, C_c, is simply estimated by

$$C_c = 0.0001 L_T C_w, \qquad \text{(E5)}$$

where

L_T = total leaf area index.

REFERENCES

Asrar, G., M. Ruchs, E. T. Kanemasu, and J. L. Hatfield, 1984: Estimating absorbed photosynthetic radiation and leaf area index from spectral reflectance in wheat. *Agron. J.,* **76,** 300–306.

Ball, J. T., 1988: An analysis of stomatal conductance. Ph.D. thesis, Stanford University, 89 pp.

Betts, A. K., J. H. Ball, A. C. M. Beljaars, M. J. Miller, and P. Viterbo, 1994: Coupling between land-surface boundary-layer parameterizations and rainfall on local and regional scales: Lessons from the wet summer of 1993. *74th Annual Meeting, Fifth Symp. on Global Change Studies,* Nashville, TN, Amer. Meteor. Soc., 174–181.

Camillo, P., and T. J. Schmugge, 1981: A computer program for the simulation of heat and moisture flow in soils. NASA Tech. Memo. 82 121, National Aeronautics and Space Administration, Greenbelt, MD, 93 pp.

——, and R. J. Gurney, 1986: A resistance parameter for bare soil evaporation models. *Soil Sci.,* **141,** 94–105.

Chang, A. T. C., J. L. Foster, and D. K. Hall, 1990: Satellite sensor estimates of Northern Hemisphere snow volume. *Int. J. Remote Sens.,* **11**(1), 167–171.

Coakley, J. A., Jr., and P. Chylek, 1975: The two-stream approximation in radiative transfer: Including the angle of incident radiation. *J. Atmos. Sci.,* **32,** 409–418.

Collatz, G. J., J. A. Berry, G. D. Farquhar, and J. Pierce, 1990: The relationship between the Rubisco reaction mechanism and models of leaf photosynthesis. *Plant Cell Environ.,* **13,** 219–225.

——, J. T. Ball, C. Grivet, and J. A. Berry, 1991: Physiological and environmental regulation of stomatal conductance, photosynthesis and transpiration: A model that includes a laminar boundary layer. *Agric. For. Meteor.,* **54,** 107–136.

——, M. Ribas-Carbo, and J. A. Berry, 1992: Coupled Photosynthesis–Stomatal Conductance Model for leaves of C_4 plants. *Aust. J. Plant Physiol.,* **19,** 519–538.

Deardorff, J. W., 1977: Efficient prediction of ground surface temperature and moisture with inclusion of a layer of vegetation. *J. Geophys. Res.,* **83,** 1889–1903.

Denmead, O. T., 1976: Temperate cereals. *Vegetation and the Atmosphere,* Vol. 2, J. L. Monteith, Ed., Academic Press, 31 pp.

Dickinson, R. E., 1983: Land surface processes and climate-surface albedos and energy balance. *Advances in Geophysics,* Academic Press, 48 pp.

——, 1984: Modeling evapotranspiration for three-dimensional global climate models. *Climate Processes and Climate Sensitivity,* J. E. Hanson and T. Takahashi, Eds., Amer. Geophys. Union, 58–72.

——, and A. Henderson-Sellers, 1988: Modeling tropical deforestation: A study of GCM land-surface parameterizations. *Quart. J. Roy. Meteor. Soc.,* **114,** 439–462.

Dorman, J. L., and P. J. Sellers, 1989: A global climatology of albedo, roughness length and stomatal resistance for atmospheric general circulation models as represented by the simple biosphere model (SiB). *J. Appl. Meteor.,* **28,** 833–855.

Farquhar, G. D., S. von Caemmerer, and J. A. Berry, 1980: A biochemical model of photosynthetic CO_2 fixation in leaves of C_3 species. *Planta,* **149,** 78–90.

Federer, C. A., 1979: A soil-plant-atmosphere model for transpiration and availability of soil water. *Water Resour. Res.,* **15.3,** 555–562.

Field, C., 1983: Allocating leaf nitrogen for the maximization of carbon gain: Leaf age as a control on the allocation program. *Oecologia,* **56,** 341–347.

——, and H. A. Mooney, 1986: The photosynthesis–nitrogen relationship in wild plants. *On the Economy of Plant Form and Function,* T. J. Givnish, Ed., Cambridge University Press, 25–55.

Garratt, J. R., 1978: Flux profile relations above tall vegetation. *Quart. J. Roy. Meteor. Soc.,* **104,** 199–211.

——, 1993: Sensitivity of climate simulations to land-surface and atmospheric boundary-layer treatments—a review. *J. Climate,* **6,** 419–449.

Goudriaan, J., 1977: *Crop Micrometeorology: A Simulation Study.* Wageningen Center for Agricultural Publishing and Documentation, 249 pp.

Hall, F. G., K. F. Huemmrich, and S. N. Goward, 1990: Use of narrow-band spectra to estimate the fraction of absorbed photosynthetically active radiation. *Remote Sens. Environ.,* **32**(1), 47–54.

——, ——, S. J. Goetz, P. J. Sellers, and J. E. Nickeson, 1992: Satellite remote sensing of surface energy balance: Success, failures and unresolved issues in FIFE. *J. Geophys. Res. FIFE Special Issue,* **97,** 19 061–19 089.

Harrison, E. F., P. Minnis, B. R. Barkstrom, V. Ramanathan, R. D. Cess, and G. G. Gibbson, 1990: Seasonal variation of cloud radiative forcing derived from the Earth Radiation Budget Experiment. *J. Geophys. Res.,* **95,** 18 687–18 703.

International Mathematical and Statistical Library (IMSL), 1984: Chapter Z, IMSL, ZXSSQ-1 to ZXSSQ-7.

Jarvis, P. G., 1976: The interpretation of the variation in leaf water potential and stomatal conductance found in canopies in the field. *Philos. Trans. Roy. Soc. London, Ser. B.,* **273,** 593–610.

Koster, R., and M. Suarez, 1992: Modeling the land surface boundary in climate models as a composite of independent vegetation stands. *J. Geophys. Res.,* **97,** 2697–2715.

——, and ——, 1994: The components of a SVAT scheme and their effects on a GCM's hydrological cycle. *Adv. Water Resour.,* **17,** 61–78.

Kuchler, A. W., 1983: World map of natural vegetation. *Goode's World Atlas,* 16th ed., Rand McNally, 16–17.

Lean, J., and D. A. Warrilow, 1989: Simulation of the regional climatic impact of Amazon deforestation. *Nature,* **342,** 411–413.

Legg, B. J., and I. F. Long, 1975: Turbulent diffusion within a wheat canopy II. *Quart. J. Roy. Meteor. Soc.,* **101,** 611–628.

Matthews, E., 1984: Prescription of land-surface boundary condition in GISS GCM II: A simple method based on high resolution

vegetation data bases. NASA Tech. Memo. 86096, National Aeronautics and Space Administration, Greenbelt, MD, 20 pp.

——, 1985: Atlas of archived vegetation, land-use and seasonal albedo data sets. NASA Tech Memo. 86199, National Aeronautics and Space Administration, Greenbelt, MD, 53 pp.

Milly, P. C., and P. S. Eagleson, 1982: Parameterization of moisture and heat fluxes across the land surface for use in atmospheric general circulation models. Rep. 279, Dept. of Engineering, Massachusetts Institute of Technology, 159 pp.

Monteith, J. L., 1973: *Principles of Environmental Physics.* Edward Arnold Ltd., 242 pp.

Myneni, R. B., G. Asrar, D. Tanre, and B. J. Choudhury, 1992: Remote sensing of solar radiation absorbed and reflected by vegetated land surface. *IEEE Trans. Geosci. Remote Sens.,* **30,** 302–314.

Nobre, C. A., P. J. Sellers, and J. Shukla, 1991: Amazonian deforestation and regional climate change. *J. Climate,* **4,** 957–988.

Noilhan, J., P. Lacarrere, and P. Bougeaul, 1991: An experiment with an advanced surface parameterization in a mesobeta-scale model III. Comparison with the HAPEX-MOBILHY dataset. *Mon. Wea. Rev.,* **119,** 2393–2413.

Paulson, C. A., 1970: Mathematical representation of wind speed and temperature profiles in the unstable atmospheric surface layer. *J. Appl. Meteor.,* **9,** 857–861.

Pielke, R. A., and R. Avissar, 1990: Influence of landscape structure on local and regional climate. *Landscape Ecol.,* **4,** 133–155.

Randall, D. A., D. A. Dazlich, C. Zhang, A. S. Denning, P. J. Sellers, C. J. Tucker, L. Bounoua, J. A. Berry, G. J. Collatz, C. B. Field, S. O. Los, C. O. Justice, and I. Fung, 1996: A revised land surface parameterization (SiB2) for GCMs. Part III: The Greening of the Colorado State University General Circulation Model. *J. Climate,* **9,** 738–763.

Raupach, M. R., and A. S. Thom, 1981: Turbulence in and above plant canopies. *Ann. Rev. Fluid Mech.,* **13,** 97–129.

Ross, J., 1975: Radiative transfer in plant communities. *Vegetation and the Atmosphere,* J. L. Monteith, Ed., Academic Press, 13–52.

Ruprecht, E., and W. M. Gray, 1976: Analysis of satellite-observed tropical cloud clusters II thermal moisture and precipitation fields. *Tellus,* **28,** 414–426.

Sato, N., P. J. Sellers, D. A. Randall, E. K. Schneider, J. Shukla, J. Kinter, Y-T Hou, and E. R. Albertazzi, 1989a: Effects of implementing the simple biosphere model (SiB) in a GCM. *J. Atmos. Sci.,* **46,** 2757–2782.

——, ——, ——, ——, ——, ——, ——, and ——, 1989b: Implementing the simple biosphere model (SiB) in a general circulation model: Methodology and results. NASA Contractor Report, NASA HQ, 79 pp. [Available from NASA HQ, Independence Avenue, Washington D.C. 20545.]

Schimel, D. S., T. G. F. Kittel, A. K. Knapp, T. R. Seastedt, W. J. Parton, and V. B. Brown, 1991: Physiological interactions along resource gradients in a tall grass prairie. *Ecology,* **72,** 672–684.

Sellers, P. J., 1985: Canopy reflectance, photosynthesis and transpiration. *Int. J. Remote Sens.,* **8,** 1335–1372.

——, 1987: Canopy reflectance, photosynthesis and transpiration. Part II: The role of biophysics in the linearity of their interdependence. *Remote Sens. Environ.,* **21,** 143–183.

——, Y. Mintz, Y. C. Sud, and A. Dalcher, 1986: A simple biosphere model (SiB) for use within general circulation models. *J. Atmos. Sci.,* **43,** 305–331.

——, J. W. Shuttleworth, J. L. Dorman, A. Dalcher, and J. M. Roberts, 1989: Calibrating the simple biosphere model (SiB) for Amazonian tropical forest using field and remote sensing data. Part I: Average calibration with field data. *J. Appl. Meteor.,* **28,** 727–759.

——, J. A. Berry, G. J. Collatz, C. B. Field, and F. G. Hall, 1992a: Canopy reflectance, photosynthesis and transpiration. Part III: A reanalysis using enzyme kinetics—electron transport models of leaf physiology. *Remote Sens. Environ.,* **42,** 187–216.

——, F. G. Hall, G. Asrar, D. E. Strebel, and R. E. Murphy, 1992b: An overview of the first ISLSCP field experiment. *J. Geophys. Res. FIFE Special Issue,* **97,** 18 345–18 372.

——, M. D. Heiser, and F. G. Hall, 1992c: Relationship between surface conductance and spectral vegetation indices at intermediate (100 m²–15 m²) length scales. *J. Geophys. Res. FIFE Special Issue,* **97,** 19 033–19 060.

——, S. O. Los, C. J. Tucker, C. O. Justice, D. A. Dazlich, G. J. Collatz, and D. A. Randall, 1996: A revised land surface parameterization (SiB2) for atmospheric GCMs. Part II: The generation of global fields of terrestrial biophysical parameters from satellite data. *J. Climate,* **9,** 706–737.

Shaw, R. H., and A. R. Pereira, 1982: Aerodynamic roughness of a plant canopy: A numerical experiment. *Agric. Meteor.,* **26,** 51–65.

Shu, F. S., 1982: Moisture and heat transport in a soil layer forced by atmospheric conditions. M.S. thesis, Dept. of Civil Engineering, University of Connecticut, 72 pp.

Shuttleworth, W. J., and Coauthors, 1984: Eddy correlation measurements of energy petition for Amazonian forest. *Quart. J. Roy. Meteor. Soc.,* **110,** 1143–1163.

Thom, A. S., 1971: Momentum absorption by vegetation. *Quart. J. Roy. Meteor. Soc.,* **97,** 414–428.

——, 1972: Momentum, mass and heat exchange of vegetation. *Quart. J. Roy. Meteor. Soc.,* **98,** 124–134.

Tucker, C. J., B. N. Holben, J. H. Elgin, and E. McMurtrey, 1981: Remote sensing of total dry matter accumulation in winter wheat. *Remote Sens. Environ.,* **11,** 171–190.

——, I. Y. Fung, C. D. Keeling, and R. H. Gammon, 1986: Relationship between atmospheric CO_2 variations and a satellite-derived vegetation index. *Nature,* **319,** 195–199.

Villalobos, F. J., and E. Fereres, 1990: Evaporation measurements beneath corn, cotton and sunflower canopies. *Agron. J.,* **82,** 1153–1159.

von Caemmerer, S., and G. D. Farquhar, 1985: Kinetics and activation of Rubisco and some preliminary modeling of RuP2 pool sizes. *Proc. of the 1983 Conf. at Tallinn,* J. Vill, G. Grishina, and A. Laisk, Eds., Estonian Academy of Sciences, 46–58.

Xue, Y., and J. Shukla, 1991: The influence of land properties on Sahel climate. Part I: Desertification. *J. Climate,* **6,** 2232–2245.

Zobler, L., 1986: A world soil file for global climate modeling. NASA Tech. Memo. 87802, National Aeronautics and Space Administration, Washington, D.C., 32 pp.